



Deep sequencing reveals the mitochondrial DNA variation landscapes of breast-to-brain metastasis blood samples

Journal:	<i>Mitochondrial DNA Part A</i>
Manuscript ID	GDNA-FLRP-2017-0109
Manuscript Type:	Full length Research Paper
Date Submitted by the Author:	18-Apr-2017
Complete List of Authors:	McGeehan, Rhiannon; University of Portsmouth, School of Pharmacy and Biomedicine Cockram, Lewis; University of Portsmouth, Institute of Biomedical and Biomolecular Science Keatley, Kathleen; University of Portsmouth, Institute of Biomedical and Biomolecular Science Eccles, Diana; University of Southampton, Faculty of Medicine An, Qian; University of Portsmouth, School of Pharmacy and Biomedicine
Keywords:	mtDNA, breast to brain metastasis, 3D protein structural mapping and analysis, breast cancer

SCHOLARONE™
Manuscripts

Deep sequencing reveals the mitochondrial DNA variation landscapes of breast-to-brain metastasis blood samples

Rhiannon E. McGeehan^{1*}, Lewis A. Cockram^{1,2§}, Kathleen Keatley^{1,3}, Diana M. Eccles⁴ and Qian An^{2*}

- ¹ Brain Tumour Research Centre, Institute of Biomedical and Biomolecular Sciences, University of Portsmouth, Portsmouth, PO1 2DT, UK
- ² School of Pharmacy and Biomedical Sciences, Institute of Biomedical and Biomolecular Sciences, University of Portsmouth, Portsmouth, PO1 2DT, UK
- ³ School of Biological Sciences, Institute of Biomedical and Biomolecular Sciences, University of Portsmouth, Portsmouth, PO1 2DT, UK
- ⁴ Cancer Sciences Academic Unit, Faculty of Medicine, University of Southampton, Somers Cancer Research Building MP824, Tremona Road, Southampton, SO16 6YA, UK
- [§] Joint first authors
- ^{*} Correspondence: rhiannon.mcgeehan@port.ac.uk or qian.an@port.ac.uk; Tel.: +44 2392842556

Abstract: Breast-to-brain metastasis (BBM) often represents a terminal event, due to the inability of many systemic treatments to cross the blood-brain barrier (BBB), rendering the brain a sanctuary site for tumour cells. Identifying genetic variations that can predict the patients who will develop BBM would allow targeting of adjuvant treatments to reduce risk while disease bulk is minimal. Germ-line genetic variations may contribute to whether a BBM forms by influencing the primary tumour sub-type that presents, or by influencing the host-response to the tumour or treatment regimen, or by facilitating transition of tumour cells across the BBB and establish a viable brain metastasis. The role of mitochondrial DNA (mtDNA) variants specifically in BBM is underexplored. Consequently, using a sensitive deep-sequencing approach, we characterised the mtDNA variation landscapes of blood samples derived from 13 females who were diagnosed with early onset breast cancer and later went on to develop BBM. We also predicted the potential pathogenic significance of variations identified in all mtDNA-encoded oxidative phosphorylation (OXPHOS) proteins using 3D protein structural mapping and analysis, to identify variations worthy of follow-up. From the 70 variations found in protein coding regions, we reveal novel links between 3 specific mtDNA variations and altered OXPHOS structure and function in 23% of the BBM samples. Further studies are required to confirm the origin of mtDNA variations, whether they correlate with 1) the predicted alterations in mitochondrial function and 2) increased risk of developing breast brain metastasis using a much larger cohort of samples.

Keywords: mtDNA; breast cancer; breast to brain metastasis; 3D protein structural mapping and analysis; OXPHOS and long PCR

1. Introduction

Breast neoplasms are currently the second highest cause of cancer related death in women. Although brain metastases are less common than lesions in the bone or lungs, they often represent a terminal event with a projected survival of just 3 to 6 months from diagnosis, with less than 20% of patients surviving more than 1 year [1–3]. Poor clinical outcome is due, in part, to the difficulty in treating the metastatic site, with systemic treatments generally being unable to penetrate the blood brain barrier. Predicting clinical outcome is also difficult due to the complicated interactions of metastatic cells with host homeostatic mechanisms, which metastatic cells ultimately exploit for their own survival and proliferation [4].

The process of brain metastasis, including breast-to-brain metastasis (BBM), consists of a series of steps. In order that a clinically relevant brain lesion is observed, tumour cells must: 1) reach >1mm³ by rapidly proliferating and establishing new vasculature, 2) invade the host cells and gain access to either the circulatory lymphatic or haematogenous systems, 3) survive the lymphatic or

haematogenous systems and arrest in the capillary beds and extravasate into the brain, and 4) proliferate and form metastasis in the brain [4]. Despite this broad understanding of the metastatic process, the incidence of BBM is on the increase and there is consequently a need for better understanding of the BBM process as well as markers that could predict which patients will develop BBM, which in turn could improve current treatments for patients with BBM.

Patient-derived blood samples are often used to identify associations between genetic variations in the germ-line and cancer prognosis [5,6]. Identifying such variations could help predict which patients may develop BBM, allowing the targeting of adjuvant treatments aimed at reducing risk while the disease bulk is minimal.

MtDNA, which exists as multiple copies in the mitochondrial matrix, is 16,569 base pairs long and encodes 37 genes. These genes provide 13 key catalytic proteins of the oxidative phosphorylation (OXPHOS) system, as well as the 2 rRNAs (12S and 16S) and 22 tRNAs vital for their synthesis. Of the 13 mtDNA-encoded proteins, 7 contribute to complex I (NADH dehydrogenase), 1 contributes to complex III (cytochrome bc₁ complex), 3 contribute to complex IV (cytochrome c oxidase) and 2 contribute to complex V (ATP synthase).

The OXPHOS system is composed of the mitochondrial respiratory chain (complexes I to IV) and ATP synthase (complex V). This system is vital for the production of cellular energy in the form of ATP and also has numerous secondary roles in other processes including calcium homeostasis [7], reactive oxygen species (ROS) production and signaling [8] and apoptosis [9,10]. Due to the importance of OXPHOS, variations in the mtDNA sequence, which can be germ-line or somatic, have the capacity to inflict profound effects on cellular function, contributing to or causing numerous human diseases (reviewed in [11]). As several hundred mtDNA molecules co-exist within a cell or tissue however, each with the capacity to hold different variations, a certain threshold must be met for a variation to exert an observable phenotypic effect [12]. The occurrence of multiple mtDNAs within a population is termed heteroplasmy.

Alterations in OXPHOS, as a consequence of mtDNA variations, have a proposed role in metastasis [13]. For example, trans-mitochondrial hybrids (cybrids), formed through the cell-cell fusion of enucleate highly metastatic lung cancer cells and mtDNA deplete lung cancer cells with low metastatic potential, enhanced the recipient cell's ability to form metastatic nodules in the lungs of mice following tail vein inoculation [14]. Consistent with this, the reciprocal mtDNA exchange suppressed the ability of the host cells to form metastatic nodules [14]. Despite the various studies that have looked into the incidence and predisposing role of mtDNA variations in primary breast cancer [15–18] and the role of mtDNA variations in the metastatic process using *in vitro* cellular and mouse xenograft models [13–14, 46], no similar studies have been conducted in the context of BBM.

As a first step towards determining whether mtDNA variations in the germ-line could influence the likelihood of developing breast to brain metastasis, in this study we determined the blood mtDNA variation landscapes of 13 breast to brain metastasis patients using an established, sensitive deep sequencing approach [19]. As expected, numerous mtDNA variations were detected relative to the revised Cambridge reference sequence (rCRS [23] [Genbank: NC_012920]). Consequently, in order to draw up a short-list of candidates worthy of follow up investigation, all of the non synonymous variations identified in mtDNA-encoded OXPHOS proteins were then inspected in detail *in silico* using the latest, best quality and homologous 3D protein structure data available to analyse and predict their potential functional impact on the OXPHOS system [20] and therefore potential links with the BBM process. Until now, this has only been possible for mtDNA-variations in complex III and IV genes [19, 20]. However, recent publication of the cryo-EM 3D structures for complexes I and V [28,29, respectively] means, for the first time, we can also gain insight into the impact of mtDNA-variations at the level of protein structure in these complexes.

2. Materials and Methods

2.1 Breast to brain metastasis patients and DNA samples

Thirteen whole blood DNA samples were obtained from a subset of the Prospective study of Outcomes in Sporadic vs Hereditary breast cancer (POSH) [21,22]. Specifically, these patients had developed breast-to-brain metastasis. Patients were aged 40 or younger, and had been diagnosed with invasive breast cancer between January 2000 and January 2008. They also had varying NPI (Nottingham prognostic index) scores, hormone receptor expression and treatment exposure (Table S1). The NPI is used to calculate the prognosis of breast cancer patients following surgery, taking into consideration the size of the lesion, the number of lymph nodes affected and the tumour grade (I-III). As a collective, the patients in this study had an average NPI score of just above 5.4, meaning 70% of patients had a projected survival of 5 years.

2.2 Long PCR amplification and sequencing of complete mtDNAs

Based on the method of Lloyd et al. 2015 [19], total DNA was extracted from the total blood of each patient using DNeasy Blood & Tissue Kit (Qiagen) according to the manufacturer's instructions. 100ng of total whole blood DNA of each patient, was amplified using two overlapping mtDNA specific primer pairs: CytbF and HumanLongR (Amplicon 1) or HumanLongF and CytbR (Amplicon 2) to yield two halves of the mitochondrial genome in each case, which were then resolved by agarose gel electrophoresis, purified and quantified (Table S2). Amplicon 1 and 2 from each sample were pooled (0.65 nM each) and 1ng of DNA from each pool was used to construct 13 Truseq Nano libraries (Illumina) which were combined, sequenced with paired-end 2 X 150 reads on the Illumina MiSeq system (Department of Biochemistry, University of Cambridge).

2.3 Identification of variations, determination of heteroplasmy and annotation

Post sequencing, reads obtained from the Illumina Resequencing Workflow (http://supportres.illumina.com/documents/documentation/software_documentation/miseqreporter/miseq-reporter-user-guide-15042295-b.pdf), were aligned against the rCRS [23] [Genbank: NC_012920] using the Burrows Wheeler Aligner (Galaxy Tools Version (GTv) 1.2.3). The rCRS, which represents haplogroup H2a2, is currently the standard sequence used for identifying the presence of mtDNA variations. Refinement of the initial alignment was then conducted through the marking and removal of duplicate reads, using Picard beta (GTv 1.56.0), followed by setting up regions for indel realignment, realignment around indels, identification of co-variables and recalibration of quality scores using the GATK tools beta (GTv 0.0.4, 0.0.6, 0.0.5 and 0.0.6, respectively).

Variant calling was carried out on the processed alignment with the GATK unified genotyper (GTv 0.0.6) to identify regions of the sequences that diverged from the rCRS. Complete processing of reads through this workflow removed the presence of several suspected false variations (G3483C, T3488A, A3492C and 3492insC), that frequently reside in the unprocessed variant files generated directly by the Illumina Resequencing Workflow.

To further minimise miscalling of variations, those which had previously been identified as "false" variants due to misalignments around homopolymer tracts or sequencing errors by Ju et al. (A302C, C309T and C3106A; [27]) were discarded. Finally, variants at sites in the rCRS which are known to contain rare alleles (A263, A750, A1438, A8860 and A15326) were not considered in further analysis [23].

To confirm the presence and calculate the heteroplasmy of each of the remaining variations a minimum read quality (Phred) score of 30 (Q30) was applied, this means that there is a very low likelihood (just a 0.01% chance) that the variations detected were due to sequencing error. To be confident that the variants called were not due to sequencing error a stringent heteroplasmy cut off of $\geq 1\%$ was applied, i.e. the number of mtDNA molecules harboring the variant had to be $\geq 1\%$ or $\leq 99\%$ to be considered heteroplasmic. If $< 1\%$ then the variant would be considered homoplasmic wild-type. If $> 99\%$ then the variant would be considered homoplasmic (pure) mutant. To determine heteroplasmy, 250 of the Q30-reads (with the duplicates removed) in the alignment were chosen at random and then heteroplasmy was calculated by dividing the depth of reads with the variant nucleotide by 250, and then expressed as a percentage. The presence of variations was further confirmed by visually inspecting the full alignments using Tablet[47]. Annotation of the identified

variations was conducted manually by inputting variations into Mitowheel (<http://mitowheel.org/mitowheel.html>) to ascertain their locus and precise position in the mitochondrial genome.

2.4 Prevalence of variations in normal/healthy (control) bloods and pathologic tissues

Previous disease associations of the variations were established through MITOMAP (<http://www.mitomap.org/MITOMAP>) and the human mitochondrial database (HmtDB; <http://www.hmtdb.uniba.it/hmtdb/>). The HmtDB was also used to determine the prevalence of variations within bloods obtained from normal, healthy individuals (as controls). The HmtDB contains over 28,196 and 3,539 mitogenomic sequences obtained from the tissues of normal, healthy subjects and patients, respectively.

2.5 Identifying functional candidates using three-dimensional protein structure mapping and analysis

Three-dimensional (3D) protein structure mapping and analysis was used to examine and predict the functional impact of all non synonymous variations identified in mitochondrial encoded proteins. This approach was developed and validated on a number of complex III and complex IV variations associated with a broad range of human diseases, and has more recently been used to identify mtDNA variations worthy of follow up investigations using *in vitro* functional assays in glioblastoma [19,20, respectively]. Subsequently, all variations found in GBM MT-CYBs and predicted to be of significance have been shown to influence complex III properties such as activity or drug-sensitivity, when individually introduced into yeast, validating the usefulness of the approach [48]. The recent high profile publications of both the mammalian complex I [28] and complex V [29] cryo-EM structures, means here, for the first time the pathogenicity of mtDNA variations within these complexes can also be predicted, something which precluded the earlier studies [19, 20].

In brief, the 13 human mitochondrial protein sequences were used to find the latest, best quality and most similar OXPHOS complex structures for complexes I, III, IV and V available from RCSB PDB (complex I – [PDB: 5LC5] (*B. taurus*) [28]; complex III – [PDB:1NTZ] (*B. taurus*) [30] & [PDB:1BE3] (*B. taurus*) [31] ; complex IV [PDB:2EIJ] (*B. taurus*) [32] and complex V [PDB:5ARA] (*B. taurus*) [29]. Similarity between human sequences and the new complex I and V models are shown in Table S3, while the others have been documented previously [20].

Relative location and conservation of variations between the human and model sequence alignments was identified using ClustalW2 [33] and then annotated with ESPript [34]. Variations were mapped to their most homologous associated structures and displayed in PyMOL (Schrödinger, LLC). In the case of complex I, maps were generated using the X-ray generated *T. thermophilus* [PDB:4HEA] model, as this was not possible using the cryo-EM generated *B. taurus* [PDB: 5LC5] model, which is not available with docked X-ray crystallographic data. Detailed analysis of the effect of variations, based on their proximity to important structural features within the models, was then performed on the most similar structures using COOT [35]. Following this, variations were classified into 1 of 5 distinct pathogenic categories: (i) frameshift, (ii) active site, (iii) binding pocket, (iv) protein interaction region or (v) non pathogenic.

3. Results and Discussion

3.1. Generation of new complete mitochondrial genomes

Long PCR and sequencing of whole blood DNA from BBM patients yielded 13 high quality new complete mitochondrial genomes (BBM1-13). Each genome was compiled from $1,626,861 \pm 196,610$ reads with a mean length of 150.2 ± 0.3 nucleotides (Table 1). These reads were then mapped against the revised Cambridge Reference Sequence (rCRS [23]), forming alignments with an average total of

1,559,947 ± 196,351 reads and a mean depth of coverage per nucleotide of 14,224 ± 1,781 over the entire mitochondrial genome (Table 1).

3.2 Highly variable mtDNA profiles

In total, 330 variations were identified across the 13 mitochondrial genomes; this consisted of 160 nucleotide positions that were found to be altered in just one or multiple samples (detailed in Table S4). The vast majority of the total variations (274/330, 83%) were nucleotide substitutions with the remaining variations being indels, including 36 insertions and 20 deletions.

The average number of variations in each sample was 25.38 ± 15.98, with most variations occurring in BBM4 and BBM8, which contained 58 and 53, respectively. BBM6, BBM7 and BBM11 contained just 11 variations each (Figure 1A). The range of heteroplasmy for each variation detected in each sample was also diverse, with no significant differences in the average heteroplasmy (72.03% ± 34.84%) observed between samples (Figure 1B). The total number of variations and average heteroplasmy observed in this small cohort of individual samples did not appear to correlate with markers known to be associated with the likelihood of developing BBM, i.e. triple negative or Her2+, or ER- (see Rostami et al. for review [36]), nor whether the patient had been exposed to radio- or chemotherapy prior to the blood DNA being taken for analysis (Table S1), despite some studies showing chemotherapies can result in mtDNA instability [37]. This prompted us to look in more detail at the specific variations present.

3.3 D-loop, mt nd4, mt-nd5 and mt cyb are variation hotspots

Variations were identified in all regions of the mtDNA genome apart from mt nd3 (Figure 2A). Variations were predominantly situated in the displacement loop (D loop), a non coding control region and known “hotspot” for mtDNA variation in many cancers [38,39], which contained 45% (149/330) of all variations.

In the coding regions, the largest number of variations (12%; 41/330) occurred in mt rnr2, which encodes for the mitochondrial 16S rRNA. Three other mitochondrial coding genes also contained a high number of variations: mt nd4 and mt nd5 (both encoding complex I subunits) each contained 5% (18/330) and mt cyb (encoding for a complex III subunit), which contained 6% (19/330) of the total variations. These patterns did not appear to be correlated with locus length (Figure 2B).

3.4 Heteroplasmy, prevalence and disease-association characteristics of recurrent variations

Seventy out of 160 variations appeared in 3 or more samples (Table S4). Thirty-two (46%) of the recurrent variations were identified in the D-loop and included: A73G, T152C, C299A, A301C, 302insC, T310C, 310insC, A16183C, C16256T, T16311C, T16326C and T16519C. The remaining 38 (54%) of the recurrent variations were present in the RNA-coding regions. The most frequently recorded variations were (in descending order of frequency): A2706G in mt rnr2, C7028T in mt co1, A11719G in mt-nd4, A12308G in mt tl2, C14766T in mt cyb, A11467G in mt nd4, G12372A in mt nd5 and G709A in mt rnr1.

Broadly speaking, the recurrent variations could be categorised into two groups (Table S4):

(1) a large group of almost 100% heteroplasmy, probably reflecting a germ-line origin. Among these, three subgroups were identified. Those which were found at a similar frequency in the bloods of BBM patients and normal subjects (A2706G, C7028T, T152C, T16311C and T16362C) and therefore unlikely to be of significance, those which were enriched by 10% or more frequent in the bloods of BBM patients than normal subjects (A11467G, G12372A, G709A, A12308G and C16256T) and therefore potentially significant, and finally, those which were depleted by ~10% or more in the bloods of BBM patients than normal subjects (A11719G, C14766T, A73G and T16519C).

(2) a small group with reasonably low average heteroplasmy (33.69 ± 29 %), which could be of either germ-line or tumour cell origin. All of the variations in this group were enriched by ~10% or more in the bloods of BBM patients when compared to normal subjects (C299A, A16183C, A301C, 302insC, T310C and 310insC) and therefore of potential significance. Interestingly, among the

somatic variations detected in primary breast cancer cells, those somatic variations detected in the “D310 repeat region of the *D-loop*”, of which *T310C* and *310insC* (this study) would be examples, have been promoted as marker for breast tumourigenesis [40]. *C16256T* has been detected in breast and brain tumours previously; *T152C*, *A11467G*, *G12372A*, *A12308G* and *A16183C* have been detected in multiple tumour types, including breast and brain tumours previously; *T16362C*, *T16519C* and *T310C* have been detected in multiple tumour types including brain tumours previously; and *A73G* and *T16311C* have been detected in multiple tumour types previously, although not breast or brain tumours. On the other hand, *A2706G*, *C7028T*, *A11719G*, *C14766T*, *G709A*, *C299A*, *A301C*, *302insC* and *310insC* have not been reported in tissues of patients with pathology previously (Table S4).

Although, there is evidence that suggests mtDNA variations can play a role in primary breast cancer, e.g. the germ-line variations: *T16189C* [15], *G9055A*, *T16519C*, *T239C* and *C16207T* [16,17] are associated with breast cancer development susceptibility and *G10398A* is associated with higher breast cancer risk in African women [18], these were not among the recurrent variations in our cohort.

3.5 Global structural maps

Overall 116 variations were identified in protein coding regions, of these 79 (68%) were synonymous and 37 (32%) were non synonymous (Figure 3A). All non-synonymous variations in the mtDNA-encoded OXPHOS genes were mapped onto their corresponding structural homologs, yielding the first insight into their distribution across the complexes. Figure 4, which is a compendium of the 23 non-synonymous variations identified in all of the BBM patients, reveals a non-uniform distribution. Most variations were found in (in descending order): complex I, IV, III and V. The high frequency of variations in complexes I, IV and III can be accounted for by variation hotspots (again in descending order) in MT-ND1 and ND5 of complex I, MT-CO3 of complex IV and MT-CYB of complex III, respectively. MT-ATP6 also contained a couple of variations, while MT-CO1, MT-CO2, MT-ND2 and MT-ND6 each contained just one variation; MT-ND3, ND4, ND4L, and MT-ATP8 (not shown), however, remained variation free. Among the non-synonymous variations, 48% (11 of 23) were conserved between the human sequences and the bovine models (Figure S1). Despite complex I containing most of the non-synonymous variations, just 30% (3 of 10) were conserved, followed by 40% in complex III (2 of 5), 60% in complex IV (4 of 6) and 100% in complex V (2 of 2)(Figure 4, Figure S1 and Table S3).

3.6 Three functional candidates identified

Owing to the 61-91% identity that exists between the human sequences and the homologs ([19] and Table S3), we were able to perform, for the first time, detailed 3D structural analysis on all complexes of the OXPHOS system containing mtDNA-encoded subunits. Using this approach, we were able to predict just 3 out of the 23 non-synonymous variations were likely to have a functional impact at the level of protein structural changes, and could be put into previously defined structural/functional classes [19,20]. One occurred in a complex III ligand/inhibitor binding pocket region (class 3) and two occurred in protein-protein interaction regions (class 4), one in complex IV and one in complex V. The remaining 9 variations, including all 10 in complex I, are predicted to be non-functional (Table 2).

The absence, or very low frequency, of all 3 of the functional candidates in the bloods of normal healthy individuals further hints that the variations could be important. According to the HmtDB: the complex IV variation (E153G) has previously been documented in diabetes, while *T14819insTTCTATA* and *S99P* have not been previously been documented were not reported (Table S4 and S5). Intriguingly, *S99P* has been reported as a somatic variant in the TCGAs-BRCA project of primary breast invasive carcinoma patients.

3.7 Mechanistic insights

The structural consequences of the 3 variations predicted to be functional are illustrated in Figures 5 and 7.

Figure 5A to D depicts the structural consequence of the 14819insTCTATA in frame insertion on the only mtDNA-encoded subunit of Complex III: MT-CYB. Complex III is at the centre of the OXPHOS system, and catalyses the transfer of electrons from ubiquinol to cytochrome c, which is coupled with the translocations of protons across the inner mitochondrial membrane. Complex III is also a major site for ROS production. MT-CYB lies at the centre of dimeric complex III, and forms intimate interactions with 20 to 22 additional subunits (10 to 11 per MT-CYB monomer) that are nuclear DNA-encoded. The subunit contains two hemes and two inhibitor binding sites, the Qo and Qi sites. Although the codons remain in register, the introduction of 6 new nucleotides at position 14819 of the mitochondrial genome eventually causes a serine to phenylalanine substitution at position 25 before the addition of a further 2 new amino acids, a tyrosine and a threonine at position 26 and 27, respectively, of the MT-CYB polypeptide (Figure S2). Although it is difficult to model the precise effects of these changes, such a substantial change is unlikely to be easily accommodated by the wild type protein (Figure 5A, C) and we predict local mis-folding of the mutant MT-CYB in a region proximal to the ubiquinol/ubiquinone binding site (the Qi-site; Figure 5B). The mis-folding could also affect the surface of MT-CYB (Figure 5C, D), disrupting its interactions with the nuclear subunits, and therefore the stability of complex III. Taken together, 14819insTCTATA is likely have an effect on complex III activity. As inhibitors can also bind to the Qi-site, this variation could also influence the efficacy of complex III inhibitors eliciting mitochondrially-mediated apoptosis.

A9664G causes the amino acid substitution E153G in MT-CO3. Complex IV, which is the terminal enzyme of the MRC that catalyses the electron transfer from cytochrome c to oxygen, which (like in complex III) is also coupled to proton translocation across the inner mitochondrial membrane. MT-CO3 forms a homodimer at the centre of complex IV. Although MT-CO3 does not house any active sites/binding pockets, through its interactions with MT-CO1 and various nuclear encoded subunits e.g. COX6A, it is thought to play a key role in the formation and therefore stabilisation of complex IV dimer [41]. In wild type MT-CO3, E153 occupies a position on the surface of MT-CO3 and interacts with alanine at position 13 of the nuclear-encoded subunit COX6A (Figure 6A). The E153G substitution is predicted to eliminate a hydrogen bond interaction (Figure 6B) that usually occurs between the large, negatively charged wild type glutamic acid residue of MT-CO3 and the smaller hydrophobic alanine of nuclear COX6A, potentially undermining the interaction between E153G and COX6A (Figure 6C, D). In summary, E153G could affect complex IV stability and therefore activity. Consistent with this view, knockdown of the subunit (although a more severe scenario than E153G) has been shown to reduce activity of complex IV [42–44].

T8821C causes an S to P substitution at position 99 of the MT-ATP6 polypeptide (Figure 7), which forms part of the F0 region of complex V. Complex V is the primary producer of ATP in eukaryotic cells, and in addition to the hydrophobic F0 region that traverses the inner mitochondrial membrane, it has a hydrophilic F1-ATPase region that protrudes like a ‘lollipop’ head into the mitochondrial matrix. In addition to MT-ATP6 (also known as the a-subunit) the F0 region is formed of an additional mtDNA-encoded subunit (MT-ATP8, also referred to as A6L-subunit), several nuclear encoded subunits (e, f, g, DAPIT, 2 hydrophobic alpha-helices of b), a proteolipid, and the c8-ring (‘rotor’). The F0 and F1 regions are linked via the subunits OSCP, d, F6 and the hydrophilic portions of subunit b, referred to as the peripheral stalk. It is proposed that complex V drives the protons that arise in the inter membrane space (IMS) as a result of MRC activity through two half-channels formed by MT-ATP6 and the ‘rotor’. In one half channel, conserved Glu58 in one of the c-subunits receives a proton from the IMS, which induces the c-ring to rotate, with the protonated Glu residues moving away from the static portions of the F0 region (the ‘stator’ which includes the two mtDNA-encoded subunits as well as components of the peripheral stalk). Once the protonated Glu residues have moved almost a full circle around the ‘rotor’, returning to the static portion of the F0 region, the other half channel provides an exit for the protons into the matrix. The resulting in deprotonation of the Glu residue, makes it ready to receive another round of protonation

via the IMS. The mechanical energy created by the rotation, is transmitted via subunits gamma, sigma and epsilon (the 'shaft'), causing conformational changes in the alpha and beta subunits (the 'blades') of the F1 region, and ultimately ATP hydrolysis (reviewed in [29]). Complex V is often referred to as a Brownian ratchet as rotation of the c-ring occurs through Brownian motion, but it is also referred to as a turbine as the enzyme has all the parts required to make a simple turbine (a rotor, stator, shaft and blades). Wild type MT-ATP6 is a 6-alpha helical bundle, whose tertiary folds are likely to be stabilised by the 12 proline residues (Figure S1). These proline-mediated kinks are likely to be indispensable for the positioning of MT-ATP6 close to the nuclear-encoded subunits of the c-ring rotor, as well as subunit b that forms part of the stator, and MT-ATP8, whose function of which is of yet unknown. The introduction of an additional proline residue, downstream of a conserved proline at position 94 of MT-ATP6 (Figure S1, Figure 7), is likely to affect thermodynamics of the whole subunit, and as a consequence, the numerous inter-helical interactions of MT-ATP6 mentioned above [45], this in turn could reduce complex V activity.

3.8 Prevalence of functional candidates in patient bloods

The detailed structural modelling suggests that altogether just 3 out of the 13 (23%) BBM patients carried a single pathogenic variation: BBM4 carries *T14819insTTCTATA* in complex III, BBM12 carries E153G in complex IV, and BBM2 carries S99P in complex V. While the possibility that D-loop, rRNA, tRNA and synonymous variations could also affect the OXPHOS function through a variety of mechanisms, the current lack of *in silico* tools available to accurately predict the structural/functional effect of such variations on OXPHOS proteins limits informative interpretation.

3.9 Summary and future prospects

Although more patients are surviving primary breast cancer, more and more are developing secondary metastases, including to the brain. Although there are existing markers that relate to the likelihood of developing BBM (e.g. triple negative or Her2+, or ER-), more needs to be done to fully understand the process of BBM and develop additional markers that predict whether a patient will develop BBM. MtDNA variations are known to play a role in various diseases, including some cancers. With ever improving and more cost-effective sequencing technologies, an increasing number of mtDNA variations are being detected that are associated with disease. However, proving their role in processes like BBM remains difficult, one reason being that it is impossible to introduce single mtDNA variations into human mtDNA and observe direct phenotypic effects.

Our focus here was two-fold: to screen the bloods of BBM patients using an established and sensitive deep sequencing approach for mtDNA variation detection (and to predict their effect on mitochondrial function using an equally established 3D structural modelling approach [19]). We reveal that the vast majority of mtDNA protein-coding variations detected in the majority of patients tested are not predicted to have a major impact on mitochondrial function. This said, 3 of the mtDNA variations detected in three of the patients were predicted to have an impact at the level of OXPHOS protein structure. The potential multiple origins of the mtDNA variations (e.g. neutrophil, monocyte, myeloid dendritic, natural killer, T and B [49], as well tumour circulating cells [4]) detected in the bloods, as well as the different selective pressures which may act upon them, however, make it difficult to fully predict their significance on the process of BBM (even if they are predicted to evoke a change on the OXPHOS system), and requires further investigation using matched primary tumour-blood-secondary tumour samples to confirm their origin. Other future work could include determining how the 3 mtDNA variations correlate with 1) the predicted alterations in mitochondrial function using *in vitro* studies and 2) with increased risk of developing breast brain metastasis using a much larger cohort of patient samples. This study also serves as a resource by highlighting a list of several mtDNA variations which are predicted to be non-functional and therefore not worthy of further investigation, which should help scientists and clinicians avoid wasting resources. Such a systematic approach of analyzing mtDNA variations could help improve

our understanding of their role in the process of BBM as well as aid the development of markers that predict whether patients develop BBM in the future.

Acknowledgments: Running costs were provided by the Institute of Biomedical and Biomolecular Science (IBBS-fund) and REL's salary was supported by the charity Brain Tumour Research. We would also like to gratefully thank John E. McGeehan for his discussion during the design of the project and comments and guidance on the structural section of this work; Geoffrey J. Pilkington and Helen L. Fillmore for the use of the Brain Tumour Research Centre facilities; Sajid Rafiq, and Will Tapper for their discussions during the design of the project, and Nikki J. Graham for providing the blood DNA samples and associated details.

Declaration of Interest: The authors declare no conflict of interest. The founding sponsors had no role in the design of the study; in the collection, analyses, or interpretation of data; in the writing of the manuscript, and in the decision to publish the results.

References

1. Berman, A.T.; Thukral, A.D.; Hwang, W.T.; Solin, L.J.; Vapiwala, N. Incidence and patterns of distant metastases for patients with early-stage breast cancer after breast conservation treatment. *Clin. Breast Cancer*. 2013, 13, 88-94.
2. Gil-Gil, M.J.; Martinez-Garcia, M.; Sierra, A.; Conesa, G.; Del Barco, S.; González-Jimenez, S.; Villà, S. Breast cancer brain metastases: A review of the literature and a current multidisciplinary management guideline. *Clin Transl Oncol*. 2014, 16, 436-46.
3. Engel, J.; Eckel, R.; Aydemir, Ü.; Aydemir, S.; Kerr, J.; Schlesinger-Raab, A.; Dirschedl, P.; Hölzel, D. Determinants and prognoses of locoregional and distant progression in breast cancer. *Int. J. Radiat. Oncol. Biol. Phys.* 2003, 55, 1186-95.
4. Fidler, IJ. The Biology of Brain Metastasis: Challenges for Therapy. *Cancer J*. 2015, 21, 284-93.
5. Khan, S.; Fagerholm, R.; Rafiq, S.; Tapper, W.; Aittomäki, K.; Liu, J.; Blomqvist, C.; Eccles, D.; Nevanlinna, H. Polymorphism at 19q13.41 predicts breast cancer survival specifically after endocrine therapy. *Clin. Cancer Res.* 2015, 21, 4086-96.
6. Fagerholm, R.; Schmidt, M.K.; Khan, S.; Rafiq, S.; Tapper, W.; Aittomäki, K.; Groco, D.; Heikkinen, T.; Muranen, T.A.; Fasching, P.A.; et al. The SNP rs6500843 in 16p13.3 is associated with survival specifically among chemotherapy-treated breast cancer patients. *Oncotarget*. 2015, 6, 7390-407.
7. Rizzuto, R.; De Stefani, D.; Raffaello, A.; Mammucari, C. Mitochondria as sensors and regulators of calcium signalling. *Nat. Rev. Mol. Cell Biol.* 2012, 13, 566-78.
8. Sena, L.A.; Chandel, N.S. Physiological roles of mitochondrial reactive oxygen species. *Mol. Cell*. 2012, 48, 158-66.
9. Jeong, S.Y.; Seol, D.W. The role of mitochondria in apoptosis. *BMB Rep.* 2008, 41, 11-22.
10. Wang, C.; Youle, R.J. The role of mitochondria in apoptosis*. *Annu. Rev. Genet.* 2009, 43, 95-118.
11. Schon, E.A.; DiMauro, S.; Hirano, M. Human mitochondrial DNA: roles of inherited and somatic mutations. *Nat. Rev. Genet.* 2012, 13, 878-90.
12. Rossignol, R.; Faustin, B.; Rocher, C.; Malgat, M.; Mazat, J.P.; Letellier, T. Mitochondrial threshold effects. *Biochem. J.* 2003, 370, 751-62.
13. Chen, E.I. Mitochondrial dysfunction and cancer metastasis. *J. Bioenerg. Biomembr.* 2012, 44, 619-22.
14. Ishikawa, K.; Takenaga, K.; Akimoto, M.; Koshikawa, N.; Yamaguchi, A.; Imanishi, H.; Nahada, K.; Honma, Y.; Hayashi, J. ROS-generating mitochondrial DNA mutations can regulate tumor cell metastasis. *Science*. 2008, 320, 661-4.
15. Wang, Y.; Liu, V.W.S.; Tsang, P.C.K.; Chiu, P.M.; Cheung, A.N.Y.; Khoo, U.S.; Nagley, P.; Ngan, H.Y.S. Microsatellite instability in mitochondrial genome of common female cancers. *Int. J. Gynecol. Cancer*. 2006, 16, 259-66.
16. Bai, R.K.; Leal, S.M.; Covarrubias, D.; Liu, A.; Wong, L.J.C. Mitochondrial genetic background modifies breast cancer risk. *Cancer Res.* 2007, 67, 4687-94.
17. Czarnecka, A.M.; Krawczyk, T.; Plak, K.; Klemba, A.; Zdrozny, M.; Arnold, R.S.; Kofler, B.; Golik, P.; Szybinska, A.; Lubinski, J.; Mossakowska, M.; Bartnik, E.; Petros, J.A. Mitochondrial genotype and breast cancer predisposition. *Oncol. Rep.* 2010, 24, 1521-34.
18. Canter, J.A.; Kallianpur, A.R.; Parl, F.F.; Millikan, R.C. Mitochondrial DNA G10398A polymorphism and invasive breast cancer in African-American women. *Cancer Res.* 2005, 65, 8028-33.

19. Lloyd, R.E.; Keatley, K.; Littlewood, D.T.J.; Meunier, B.; Holt, W.V.; An, Q.; Higgins, S.C.; Polyzoidis, S.; Stephenson, K.F.; Ashkan, K.; Fillmore, H.L.; Pilkington, G.J.; McGeehan, J.E. Identification and functional prediction of mitochondrial complex III and IV mutations associated with glioblastoma. *Neuro-oncology*. 2015, 17, 942–52.
20. Lloyd, R.E.; McGeehan, J.E. Structural Analysis of Mitochondrial Mutations Reveals a Role for Bigenomic Protein Interactions in Human Disease. *PLoS One*. 2013, 8, e69003.
21. Eccles, D.; Gerty, S.; Simmonds, P.; Hammond, V.; Ennis, S.; Altman, D.G. Prospective study of Outcomes in Sporadic versus Hereditary breast cancer (POSH): study protocol. *BMC Cancer*. 2007, 7, 160.
22. Rafiq, S.; Tapper, W.; Collins, A.; Khan, S.; Politopoulos, I.; Gerty, S.; Blomqvist, C.; Couch, F.J.; Nevanlinna, H.; Liu, J.; Eccles, D. Identification of inherited genetic variations influencing prognosis in early-onset breast cancer. *Cancer Res*. 2013, 73, 1883–91.
23. Andrews, R.M.; Kubacka, I.; Chinnery, P.F.; Lightowlers, R.N.; Turnbull, D.M.; Howell, N. Reanalysis and revision of the Cambridge reference sequence for human mitochondrial DNA. *Nat. Genet*. 1999, 23, 147.
24. Li, H.; Durbin, R. Fast and accurate short read alignment with Burrows-Wheeler transform. *Bioinformatics*. 2009, 25, 1754–60.
25. McKenna, A.; Hanna, M.; Banks, E.; Sivachenko, A.; Cibulskis, K.; Kernysky, A.; Garimella, K.; Altshuler, D.; Gabriel, S.; Daly, M.; DePristo, M.A. The genome analysis toolkit: A MapReduce framework for analyzing next-generation DNA sequencing data. *Genome Res*. 2010, 20, 1297–303.
26. DePristo, M.A.; Banks, E.; Poplin, R.; Garimella, K.V.; Maguire, J.R.; Hartl, C.; Philippakis, A.A.; del Angel, G.; Rivas, M.A.; Hanna, M.; et al. A framework for variation discovery and genotyping using next-generation DNA sequencing data. *Nat. Genet*. 2011, 43, 491–8.
27. Ju, Y.S.; Alexandrov, L.B.; Gerstung, M.; Martincorena, I.; Nik-Zainal, S.; Ramakrishna, M.; Davies, H.R.; Papaemmanuil, E.; Gundem, G.; Shlien, A.; et al. Origins and functional consequences of somatic mitochondrial DNA mutations in human cancer. *Elife*. 2014, 3, e02935.
28. Zhu, J.; Vinothkumar, K.R.; Hirst, J. Structure of mammalian respiratory complex I. *Nature*. 2016, 536, 354–8.
29. Zhou, A.; Rohou, A.; Schep, D.G.; Bason, J.V.; Montgomery, M.G.; Walker, J.E.; Grigorieffniko, N.; Rubinstein, J.L. Structure and conformational states of the bovine mitochondrial ATP synthase by cryo-EM. *Elife*. 2015, 4, e10180.
30. Gao, X.; Wen, X.; Esser, L.; Quinn, B.; Yu, L.; Yu, C.A.; Xia, D. Structural Basis for the Quinone Reduction in the bc1 Complex: A Comparative Analysis of Crystal Structures of Mitochondrial Cytochrome bc1 with Bound Substrate and Inhibitors at the Qi Site. *Biochemistry*. 2003, 42, 9067–80.
31. Iwata, S.; Lee, J.W.; Okada, K.; Lee, J.K.; Iwata, M.; Rasmussen, B.; Link, T.A.; Ramaswamy, S.; Jap, B.K. Complete structure of the 11-subunit bovine mitochondrial cytochrome bc1 complex. *Science*. 1998, 281, 64–71.
32. Muramoto, K.; Hirata, K.; Shinzawa-Itoh, K.; Yoko-o, S.; Yamashita, E.; Aoyama, H.; Tsukihara, T.; Yoshikawa, S. A histidine residue acting as a controlling site for dioxygen reduction and proton pumping by cytochrome c oxidase. *Proc. Natl. Acad. Sci. U.S.A.* 2007, 104, 7881–6.
33. Larkin, M.; Blackshields, G.; Brown, N.; Chenna, R.; McGettigan, P.; McWilliam, H.; Valentin, F.; Wallace, I.M.; Wilm, A.; Lopez, R.; Thompson, J.D.; Gibson, T.J.; Higgins, D.G. ClustalW and ClustalX version 2. *Bioinformatics*. 2007, 23, 2947–8.
34. Gouet, P.; Courcelle, E.; Stuart, D.I.; Metoz, F. ESPript: analysis of multiple sequence alignments in PostScript. *Bioinformatics*. 1999, 15, 305–8.
35. Emsley, P.; Lohkamp, B.; Scott, W.G.; Cowtan, K. Features and development of Coot. *Acta. Crystallogr. Sect. D Biol. Crystallogr*. 2010, 66, 486–501.
36. Rostami, R.; Mittal, S.; Rostami, P.; Tavassoli, F.; Jabbari, B. Brain metastasis in breast cancer: a comprehensive literature review. *J. Neurooncol*. 2016, 127, 407–14.
37. Wiseman, H.; Halliwell, B. Damage to DNA by reactive oxygen and nitrogen species: role in inflammatory disease and progression to cancer. *Biochem. J*. 1996, 313, 17–29.
38. Akouchekian, M.; Houshmand, M.; Hemati, S.; Ansari-pour, M.; Shafa, M. High rate of mutation in mitochondrial DNA displacement loop region in human colorectal cancer. *Dis. Colon Rectum*. 2009, 52, 526–30.
39. Fliss, M.S.; Usadel, H.; Caballero, O.L.; Wu, L.; Buta, M.R.; Eleff, S.M.; Jen, J.; Sidransky, D. Facile detection of mitochondrial DNA mutations in tumors and bodily fluids. *Science*. 2000, 287, 2017–9.

40. Parrella, P.; Xiao, Y.; Fliss, M.; Sanchez-Cespedes, M.; Mazzarelli, P.; Rinaldi, M.; Nicol, T.; Gabrielson, E.; Cuomo, D.; Cohen, D.; et al. Detection of mitochondrial DNA mutations in primary breast cancer and fine-needle aspirates. *Cancer Res.* 2001, 61, 7623-6.

41. Sedláč, E.; Robinson, N.C. Sequential dissociation of subunits from bovine heart cytochrome c oxidase by urea. *Biochemistry.* 2009, 48, 8143-50.

42. Quintens, R.; Singh, S.; Lemaire, K.; de Bock, K.; Granvik, M.; Schraenen, A.; Vroegrijk, I.O.C.M.; Costa, V.; van Noten, P.; Lambrechts, D.; et al. Mice Deficient in the Respiratory Chain Gene Cox6a2 Are Protected against High-Fat Diet-Induced Obesity and Insulin Resistance. *PLoS One.* 2013, 8, e56719.

43. Tamiya, G.; Makino, S.; Hayashi, M.; Abe, A.; Numakura, C.; Ueki, M.; Tanaka, A.; Ito, C.; Tohimori, K.; Ogawa, N.; et al. A mutation of COX6A1 causes a recessive axonal or mixed form of Charcot-Marie-Tooth disease. *Am. J. Hum. Genet.* 2014, 95, 294-300.

44. Fornuskova, D.; Stiburek, L.; Wenchich, L.; Vinsova, K.; Hansikova, H.; Zeman, J. Novel insights into the assembly and function of human nuclear-encoded cytochrome c oxidase subunits 4, 5a, 6a, 7a and 7b. *Biochem. J.* 2010, 428, 363-74.

45. Schmidt, T.; Situ, A.J.; Ulmer, T.S. Structural and thermodynamic basis of proline-induced transmembrane complex stabilization. *Sci Rep.* 2016, 6, 29809.

46. Kenny TC, Hart P, Ragazzi M, Sersinghe M, Chipuk J, Sagar MA, Eliceiri KW, LaFramboise T, Grandhi S, Santos J, Riar AK, Papa L, D'Aurello M, Manfredi G, Bonini MG, Germain D. Selected mitochondrial DNA landscapes activate the SIRT3 axis of the UPR(mt) to promote metastasis. *Oncogene.* 2017 Apr 3. doi: 10.1038/onc.2017.52. [Epub ahead of print] PubMed PMID: 28368421.

47. Milne I, Stephen G, Bayer M, Cock PJ, Pritchard L, Cardle L, Shaw PD, Marshall D. Using Tablet for visual exploration of second-generation sequencing data. *Brief Bioinform.* 2013 Mar;14(2):193-202.

48. Song Z, Laleve A, Vallières C, McGeehan JE, Lloyd RE, Meunier B. Human Mitochondrial Cytochrome b Variants Studied in Yeast: Not All Are Silent Polymorphisms. *Hum Mutat.* 2016 Sep;37(9):933-41.

49. Zhang P, Samuels DC, Wang J, Zhao S, Shyr Y, Guo Y. Mitochondria single nucleotide variation across six blood cell types. *Mitochondrion.* 2016 May;28:16-22.

Supplementary Materials: Figure S1. Location of non-synonymous amino acid substitution sites following the alignments of human (rCRS) against the bovine homologous mtDNA-encoded polypeptide sequences. Figure S2. Comparison of the wild type *mt-cyb* and MT-CYB sequences against the variant sequences which contain a 6-nucleotide insertion at position 14819. Table S1: Details of the breast-to-brain metastasis patients from which whole-blood mitochondrial genomes were derived. Table S2. Long PCR Primer details. Table S3. Similarity of human sequences vs the homologous structural models used to analyse the effect mtDNA-encoded OXPHOS variations identified in breast-to-brain metastasis bloods. Table S4. Details of each mtDNA variation identified in breast-brain metastasis blood samples including location, average heteroplasmy and prevalence. Table S5. Reported disease associations of each mtDNA variation identified from breast-to-brain metastasis patient bloods.

Tables with captions

Table 1. Summary of sequencing read statistics used to generate new complete breast-to-brain metastasis blood mtDNAs.

Sample ID	Total number of reads	Number of reads mapped	Mean read length	Reads Mapped (%)	Mean DOC/nt
BBM1	1286809	1236479	150	96	11255
BBM2	1652912	1590565	150	96	14471
BBM3	1398435	1341546	151	96	12236
BBM4	1733369	1656272	150	96	15133
BBM5	1606805	1486669	150	93	13587
BBM6	2080624	2034506	150	98	18515
BBM7	1616133	1576150	150	98	14358
BBM8	1540641	1468502	151	95	13398
BBM9	1709391	1632630	150	96	14911
BBM10	1796414	1737453	150	97	15804
BBM11	1517582	1461889	150	96	13331
BBM12	1709260	1607356	150	94	14655
BBM13	1500821	1449294	150	97	13252
Average	1626861	1559947	150.2	96	14223.6
Standard Deviation	196609	196351	0.3	1.4	1781.3

Abbreviation: nt - nucleotide, DOC - depth of coverage

Table 2. Heteroplasmy, prevalence of non-synonymous variations in the mtDNA complex genes identified within the mtDNA landscapes of breast-to-brain blood samples.

Locus	Specific Nucleotide Variant	Amino Acid change	Average heteroplasmy (% \pm SD)	% Hmt DB	% BBM	Specific Sample IDs (BBM)
MT-ND1	A3796G	T164A	99.6*	0.6	7.7	6
MT-ND1	C3992T	T229M	99.2*	0.8	7.7	10
MT-ND1	A4024G	T240A	99.2*	0.7	7.7	10
MT-ND1	T4216C	Y304H	99.4 \pm 0.3*	10.5	15.4	1 and 12
MT-ND2	A4917G	N150D	98.6 \pm 0.9*	5.2	15.4	1 and 12
MT-ND5	A12397G	T21A	99.6*	0.5	7.7	5
MT-ND5	C12557T	T74I	98.4*	0.3	7.7	4
MT-ND5	G13813A	V493I	99.6*	0.1	7.7	5
MT-ND5	G13889A	C518Y	99.6*	0.1	7.7	10
MT-ND6	A14582G	V31A	99.6*	0.6	7.7	10
MT-CYB	C14766T	T7I	98.9 \pm 0.8*	74.9	46.2	1/ 4/ 8/ 9/ 12/ 13
MT-CYB	A14793G	H16R	99.6 \pm 0.0*	2.3	15.4	9 and 13
MT-CYB	T14819insTTCTA TA	S25	2.4	-	7.7	12
MT-CYB	A15218G	T158A	100 \pm 0.0*	2	7.7	9
MT-CYB	C15452A	L236I	99.4 \pm 0.9*	9.8	15.4	1 and 12
MT-CO1	G6267A	A122T	98.8*	0.2	7.7	2
MT-CO2	T8265C	L227P	24.8	0	7.7	4
MT-CO3	C9469T	T88I	100*	0.1	7.7	13
MT-CO3	G9477A	V91I	99.8 \pm 0.3*	4.2	15.4	9 and 13
MT-CO3	A9664G	E153G	98.8*	0.1	7.7	4
MT-CO3	A9667G	N154S	99.2*	0.7	7.7	9
MT-ATP6	T8821C	S99P	83.2	0	7.7	2

MT-ATP6	G8989A	A155T	97.2	0	7.7	12
---------	--------	-------	------	---	-----	----

Grey shading indicates variation classed as functional at the level of protein structural changes. The unshaded variations are classified as non-functional. %hmtDB and %BBM indicate prevalence in the human mitochondrial database and BBM cohort (this study), respectively. *Signifies homoplasmic (pure) mutant (see materials and methods).

For Peer Review Only

Figures with captions

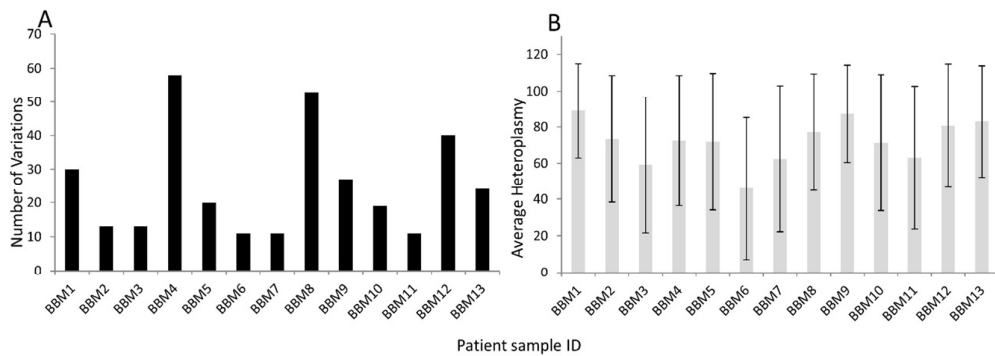


Figure 1. Total number (A) and average heteroplasmy (B) of mtDNA variations in breast-to-brain metastasis patient blood mtDNAs. Error bars indicate standard deviation.

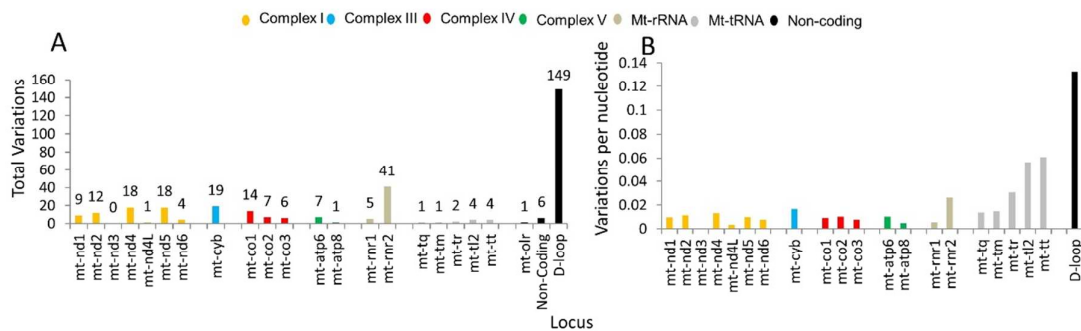


Figure 2. Presence of variations in breast-to-brain metastasis patient blood across mtDNA loci. (A) Total number of mtDNA variations identified in both coding and non-coding loci. (B) Total number of variations expressed per nucleotide in each of the mtDNA loci.

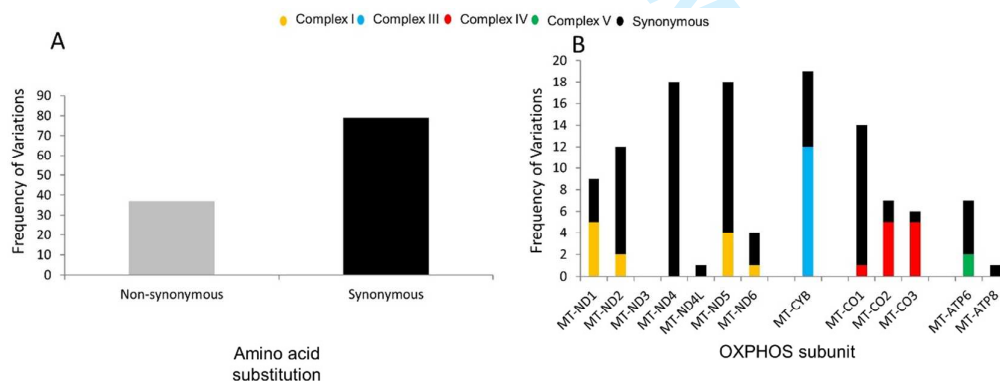


Figure 3. Pattern of synonymous and non-synonymous mtDNA variations in breast-to-brain blood mtDNAs. (A) Total and (B) across loci.

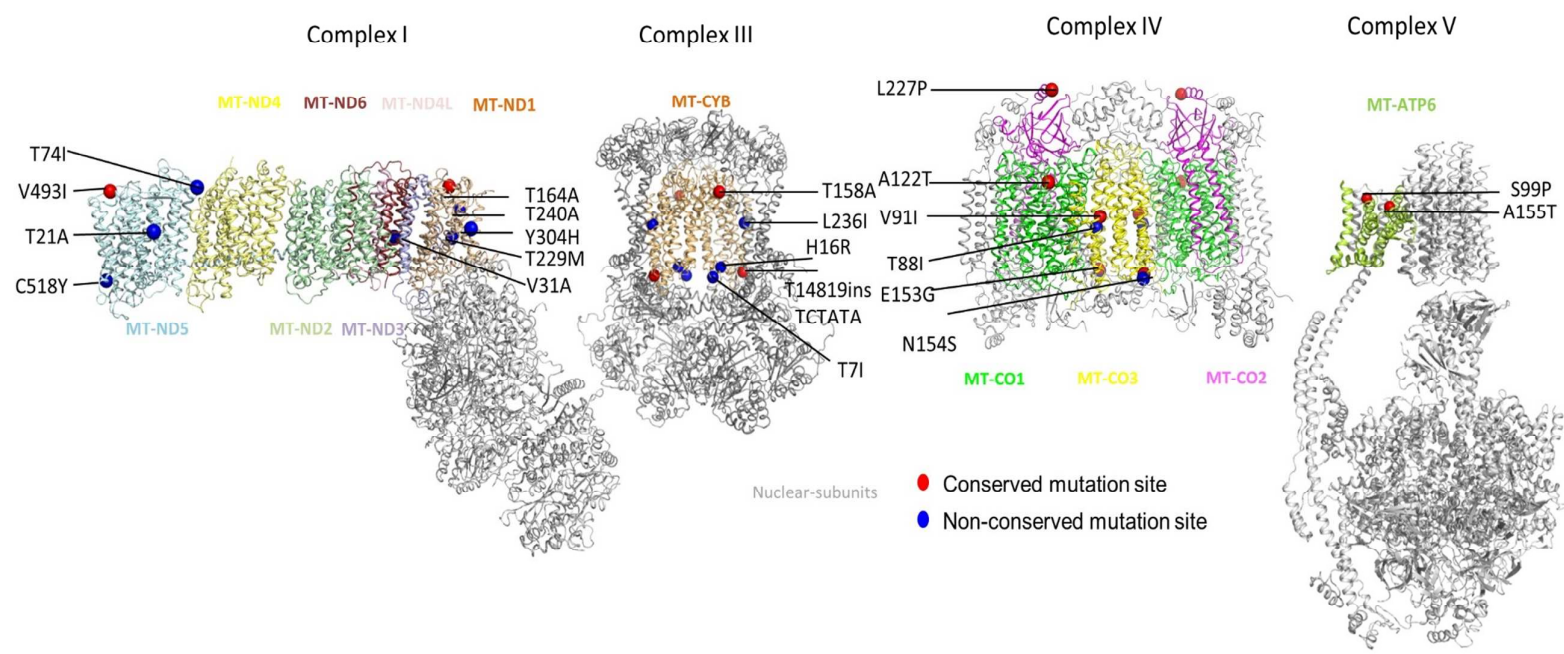


Figure 4 . Global

map of non-synonymous variations identified in the mitochondrial OXPHOS proteins of breast-to-brain metastasis patient blood mtDNAs. Variations mapped to T. thermophilus complex I homologues [PDB:4HEA], B. taurus complex III homologue [PDB:1BE3], B. taurus complex IV homologue [PDB:2EIJ] and B. taurus complex V homologue [PDB: 5ARA]. The carbon alphas of residues that are conserved and non-conserved between the human sequences and the bovine models are highlighted as red and blue spheres respectively, including for complex I eventhough the T. thermophilus structure is shown. The conserved residue N150D is not shown as there is no equivalent residue present in 4HEA

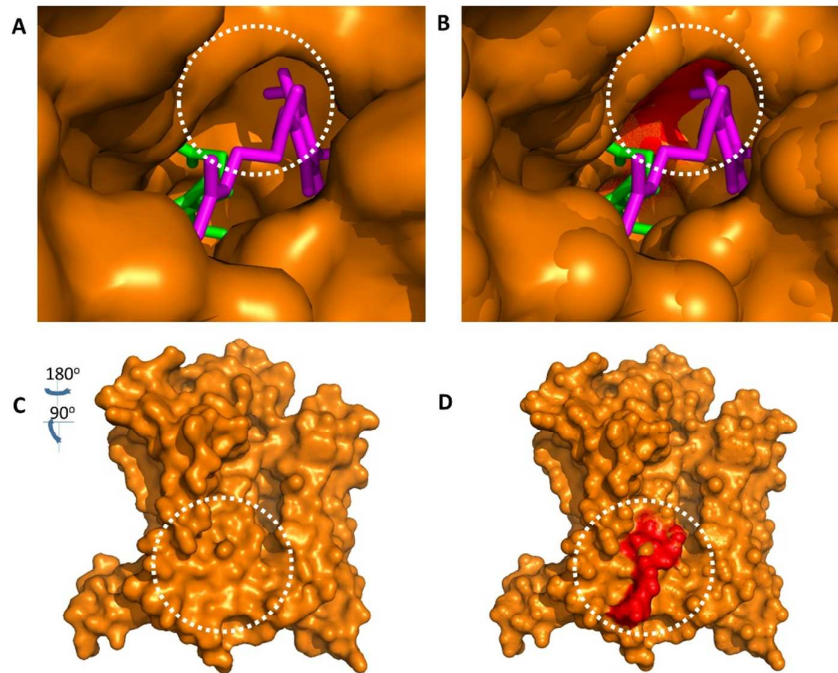


Figure 5. Structural consequences of the class 3 binding pocket variation 14819insTCTATA. The variation causes a serine to phenylalanine substitution and the addition of two amino acids at positions 25-27 of the complex III protein MT-CYB. MT-CYB is rendered as a space filling model (orange), with (A) the wild type Qi-site shown with the deeply buried heme (green) and bound ubiquinone (magenta; PDB 1NTZ). (B) The amino acid changes induced by the variation occur in the vicinity of the Qi-site (in red). (C) The surface of the wild type MT-CYB monomer. (D) The variant is likely to cause local mis-folding of MT-CYB (in red), disrupting its interaction with surrounding nuclear encoded subunits. Such changes to the MT-CYB Qi-site and surface are likely to interfere with ubiquinone/ubiquinol binding, and ultimately complex III activity.

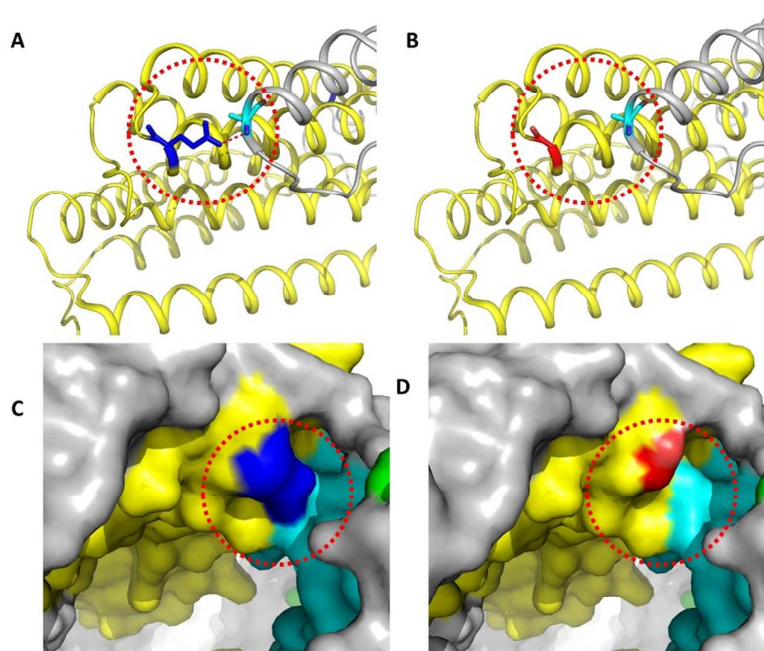


Figure 6. Structural consequences of the class 4 interaction variation A9664G. (A) Wild type E153 (blue sticks) in MT-CO3 (yellow ribbons) forms an interaction with A13 (cyan sticks) in COX6A (grey ribbon). (B) The variant G153 (red sticks) results in the loss of a hydrogen bond with A13. (C) The wild type MT-CO3 is shown as a surface model, showing E153 (blue) forms a tight interaction with A13 of COX6A (cyan). (D) Surface illustration of variant G153 (red), which no longer interacts with COX6A, which could affect the stability of complex IV.

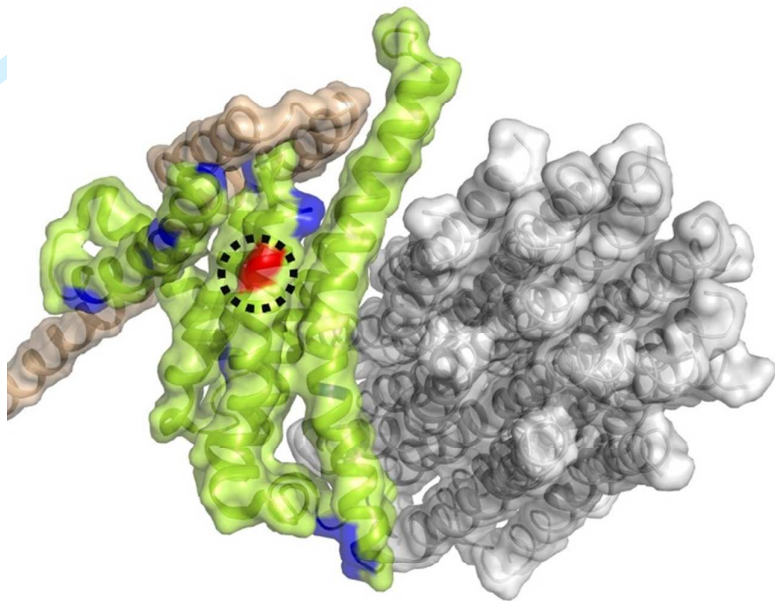


Figure 7. Structural consequences of the class 4 variation T8821C. Wild type MT-ATP6 (light green) is shown as a surface model and is formed of six kinked alpha-helices that stabilise the subunit and allow it to form intricate inter-helical interactions with subunit b (wheat), MT-ATP8 (not shown) and the c-ring (grey). Together with the hydrophobic portions of subunit b and MT-ATP8, MT-ATP6 form the static part of the F0 region, with the c-ring forming the rotary portion. It is likely that several proline residues (blue), conserved between the human sequence and the bovine model, are responsible for the kinks observed in MT-ATP6. The substitution of a serine for a proline (red) at position 99 in one of the helices, is likely to interfere with tertiary fold and destabilise the protein and disrupt its interactions, influencing complex V activity.

Table 1. Summary of sequencing read statistics used to generate new complete breast-to-brain metastasis blood mtDNAs.

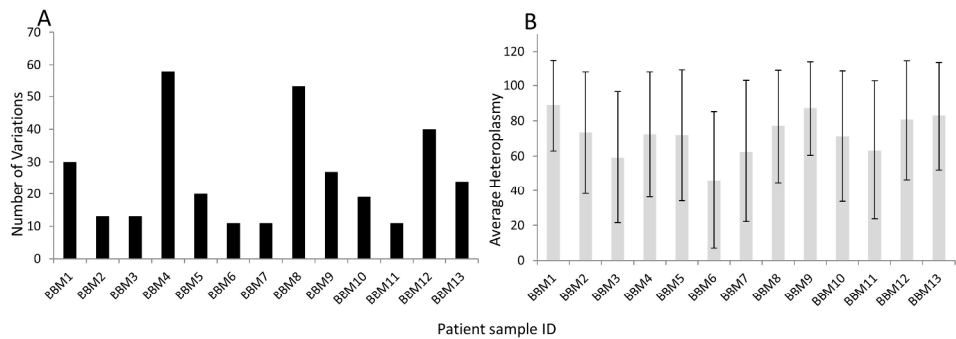
Sample ID	Total number of reads	Number of reads mapped	Mean read length	Reads Mapped (%)	Mean DOC/nt
BBM1	1286809	1236479	150	96	11255
BBM2	1652912	1590565	150	96	14471
BBM3	1398435	1341546	151	96	12236
BBM4	1733369	1656272	150	96	15133
BBM5	1606805	1486669	150	93	13587
BBM6	2080624	2034506	150	98	18515
BBM7	1616133	1576150	150	98	14358
BBM8	1540641	1468502	151	95	13398
BBM9	1709391	1632630	150	96	14911
BBM10	1796414	1737453	150	97	15804
BBM11	1517582	1461889	150	96	13331
BBM12	1709260	1607356	150	94	14655
BBM13	1500821	1449294	150	97	13252
Average	1626861	1559947	150.2	96	14223.6
Standard Deviation	196609	196351	0.3	1.4	1781.3

Abbreviation: nt - nucleotide, DOC - depth of coverage

Table 2. Heteroplasmy, prevalence of non-synonymous variations in the mtDNA complex genes identified within the mtDNA landscapes of breast-to-brain blood samples.

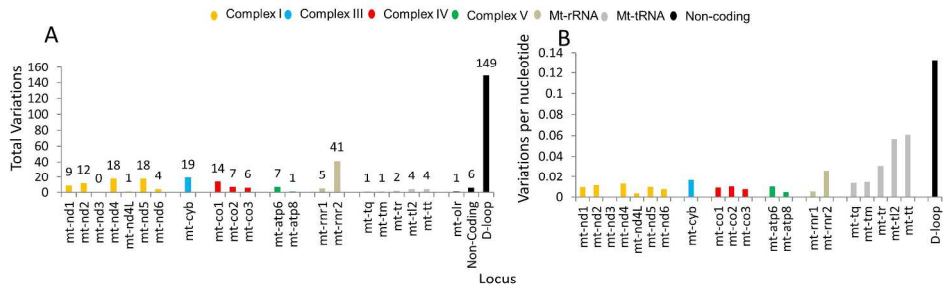
Locus	Specific Nucleotide Variant	Amino Acid change	Average heteroplasmy (% \pm SD)	% Hmt DB	% BBM	Specific Sample IDs (BBM)
MT-ND1	A3796G	T164A	99.6*	0.6	7.7	6
MT-ND1	C3992T	T229M	99.2*	0.8	7.7	10
MT-ND1	A4024G	T240A	99.2*	0.7	7.7	10
MT-ND1	T4216C	Y304H	99.4 \pm 0.3*	10.5	15.4	1 and 12
MT-ND2	A4917G	N150D	98.6 \pm 0.9*	5.2	15.4	1 and 12
MT-ND5	A12397G	T21A	99.6*	0.5	7.7	5
MT-ND5	C12557T	T74I	98.4*	0.3	7.7	4
MT-ND5	G13813A	V493I	99.6*	0.1	7.7	5
MT-ND5	G13889A	C518Y	99.6*	0.1	7.7	10
MT-ND6	A14582G	V31A	99.6*	0.6	7.7	10
MT-CYB	C14766T	T7I	98.9 \pm 0.8*	74.9	46.2	1/ 4/ 8/ 9/ 12/ 13
MT-CYB	A14793G	H16R	99.6 \pm 0.0*	2.3	15.4	9 and 13
MT-CYB	T14819insTTCTA TA	S25	2.4	-	7.7	12
MT-CYB	A15218G	T158A	100 \pm 0.0*	2	7.7	9
MT-CYB	C15452A	L236I	99.4 \pm 0.9*	9.8	15.4	1 and 12
MT-CO1	G6267A	A122T	98.8*	0.2	7.7	2
MT-CO2	T8265C	L227P	24.8	0	7.7	4
MT-CO3	C9469T	T88I	100*	0.1	7.7	13
MT-CO3	G9477A	V91I	99.8 \pm 0.3*	4.2	15.4	9 and 13
MT-CO3	A9664G	E153G	98.8*	0.1	7.7	4
MT-CO3	A9667G	N154S	99.2*	0.7	7.7	9
MT-ATP6	T8821C	S99P	83.2	0	7.7	2
MT-ATP6	G8989A	A155T	97.2	0	7.7	12

Grey shading indicates variation classified as functional at the level of protein structural changes. The unshaded variations are classified as non-functional. %hmtDB and %BBM indicate prevalence in the human mitochondrial database and BBM cohort (this study), respectively. *Signifies homoplasmic (pure) mutant (see materials and methods).



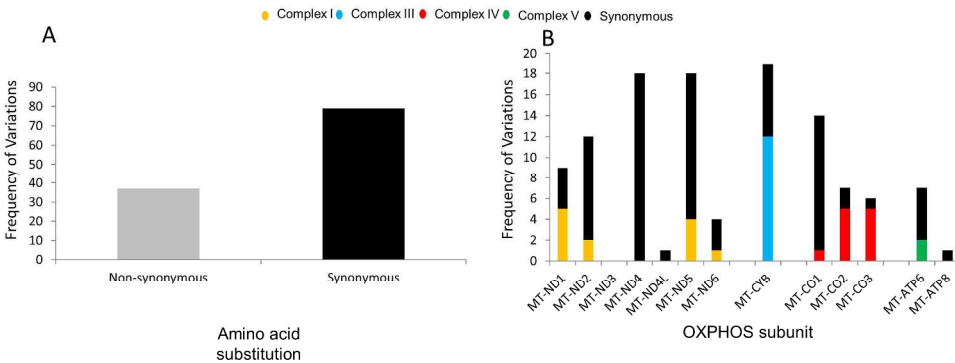
Total number (A) and average heteroplasmy (B) of mtDNA variations in breast-to-brain metastasis patient blood mtDNAs. Error bars indicate standard deviation.

254x190mm (300 x 300 DPI)



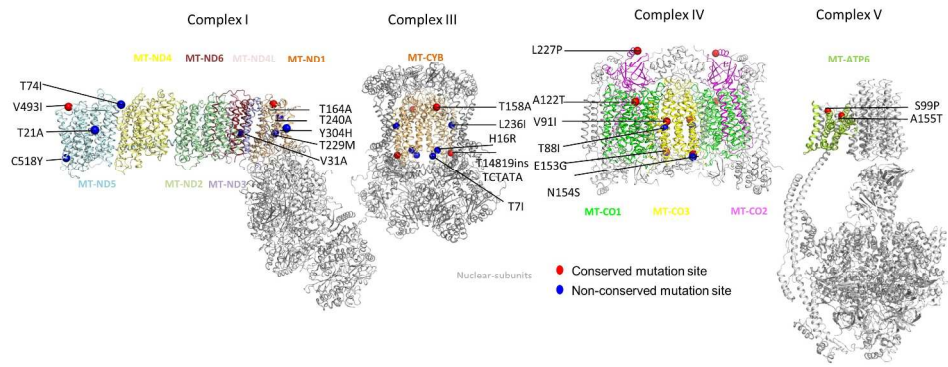
. Presence of variations in breast-to-brain metastasis patient blood across mtDNA loci. (A) Total number of mtDNA variations identified in both coding and non-coding loci. (B) Total number of variations expressed per nucleotide in each of the mtDNA loci.

254x190mm (300 x 300 DPI)



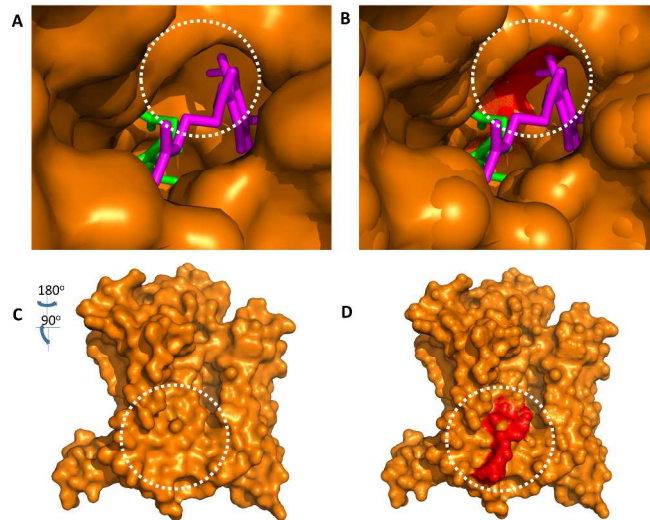
Pattern of synonymous and non-synonymous mtDNA variations in breast-to-brain blood mtDNAs. (A) Total and (B) across loci.

254x190mm (300 x 300 DPI)



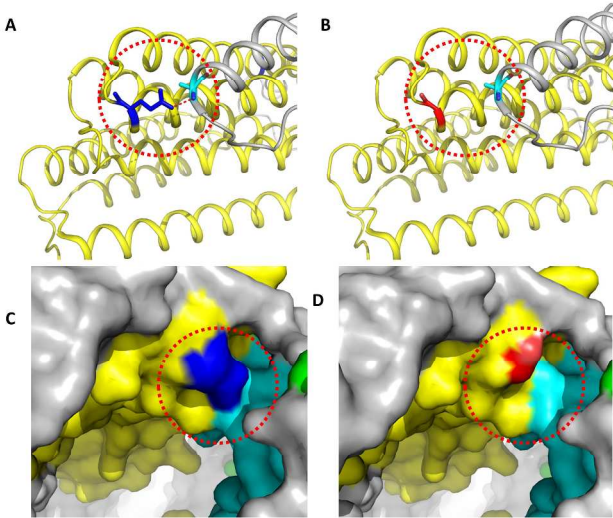
Global map of non-synonymous variations identified in the mitochondrial OXPHOS proteins of breast-to-brain metastasis patient blood mtDNAs. Variations mapped to *T. thermophilus* complex I homologues [PDB:4HEA], *B. taurus* complex III homologue [PDB:1BE3], *B. taurus* complex IV homologue [PDB:2EIJ] and *B. taurus* complex V homologue [PDB: 5ARA]. The carbon alphas of residues that are conserved and non-conserved between the human sequences and the bovine models are highlighted as red and blue spheres respectively, including for complex I eventhough the *T. thermophilus* structure is shown. The conserved residue N150D is not shown as there is no equivalent residue present in 4HEA.

254x190mm (300 x 300 DPI)



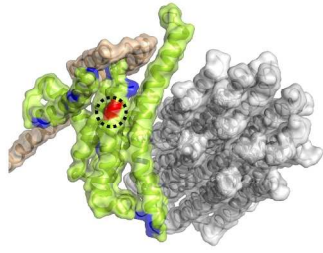
. Structural consequences of the class 3 binding pocket variation 14819insTCTATA. The variation causes a serine to phenylalanine substitution and the addition of two amino acids at positions 25-27 of the complex III protein MT-CYB. MT-CYB is rendered as a space filling model (orange), with (A) the wild type Qi-site shown with the deeply buried heme (green) and bound ubiquinone (magenta; PDB 1NTZ). (B) The amino acid changes induced by the variation occur in the vicinity of the Qi-site (in red). (C) The surface of the wild type MT-CYB monomer. (D) The variant is likely to cause local mis-folding of MT-CYB (in red), disrupting its interaction with surrounding nuclear encoded subunits. Such changes to the MT-CYB Qi-site and surface are likely to interfere with ubiquinone/ubiquinol binding, and ultimately complex III activity.

338x190mm (300 x 300 DPI)



Structural consequences of the class 4 interaction variation A9664G. (A) Wild type E153 (blue sticks) in MT-CO3 (yellow ribbons) forms an interaction with A13 (cyan sticks) in COX6A (grey ribbon). (B) The variant G153 (red sticks) results in the loss of a hydrogen bond with A13. (C) The wild type MT-CO3 is shown as a surface model, showing E153 (blue) forms a tight interaction with A13 of COX6A (cyan). (D) Surface illustration of variant G153 (red), which no longer interacts with COX6A, which could affect the stability of complex IV.

338x190mm (300 x 300 DPI)



Structural consequences of the class 4 variation T8821C. Wild type MT-ATP6 (light green) is shown as a surface model and is formed of six kinked alpha-helices that stabilise the subunit and allow it to form intricate inter-helical interactions with subunit b (wheat), MT-ATP8 (not shown) and the c-ring (grey). Together with the hydrophobic portions of subunit b and MT-ATP8, MT-ATP6 form the static part of the F₀ region, with the c-ring forming the rotary portion. It is likely that several proline residues (blue), conserved between the human sequence and the bovine model, are responsible for the kinks observed in MT-ATP6. The substitution of a serine for a proline (red) at position 99 in one of the helices, is likely to interfere with tertiary fold and destabilise the protein and disrupt its interactions, influencing complex V activity.

338x190mm (300 x 300 DPI)

1
2
3
4
5
6
7
8
9
10
11
12
13
14
15
16
17
18
19
20
21
22
23
24
25
26
27
28
29
30
31
32
33
34
35
36
37
38
39
40
41
42
43
44
45
46
47
48
49
50
51
52
53
54
55
56
57
58
59
60

Supplementary Figures and Tables

For Peer Review Only

Table S1. Details of the breast-to-brain metastasis patients from which whole-blood mitochondrial genomes were derived.

Sample ID	POSSH Sample No	NPI Score	ER	HER2	PR	BRCA status	Chemotherapy*	Adjuvant Radiotherapy*
BBM1	2003080226	5.7	negative	negative	negative	BRCA1	FEC, 6 cycles	No
BBM2	2003120358	4	positive	positive	positive	unknown	No	No
BBM3	2004070684	3.6	negative	not done	positive	unknown	No	No
BBM4	2004080723	N/A	negative	negative	negative	NMF	No	No
BBM5	2005041135	5	negative	not done	negative	unknown	FEC, 6 cycles	Yes
BBM6	2005041147	5	positive	negative	not done	unknown	EC + Docetaxel, 8 cycles	No
BBM7	2008042970	7	positive	positive	not done	unknown	FEC + Docetaxel, 6 cycles	No
BBM8	2005051216	7	positive	positive	negative	NMF	EC + Paclitaxel, 8 cycles	Yes
BBM9	2006021768	6	positive	negative	not done	unknown	FEC, 6 cycles	Yes
BBM10	2007012323	5	positive	negative	negative	unknown	E-CMF, 8 cycles	No
BBM11	2007072618	5	positive	negative	negative	unknown	E-CMF, 8 cycles	No
BBM12	2008022929	7	positive	positive	positive	unknown	EC + Docetaxel, 8 cycles	No
BBM13	2008073036	5	negative	positive	negative	unknown	FEC, 6 cycles and Docetaxel + Trastuzumab, 6 cycles	No

Abbreviations: NPI - Nottingham Prognostic index; NMF-no mutation found; ER-oestrogen receptor status; HER2-HER2 status; PR-progesterone receptor status. FEC-fluorouracil, epirubicin and cyclophosphamide; E-CMF - epirubicin, cyclophosphamide, methotrexate and fluorouracil; EC - epirubicin and cyclophosphamide. *Prior to blood samples being taken.

Table S2. Long PCR Primer details

Name	Gene	Nucleotide position	Sequence (5'-3')	Amplicon length (bp)
CytbF	<i>Mt-cyb_mt-col</i>	15029-15049	TTCCTACACATCGGGCGAGG	8573
Human			CCTCCTATGATGGCAAATACAG	
LongR		7053-7078	CTCC	
HumanLong	<i>Mt-col_mt-cyb</i>		AGGAGACCCCATTCTATACCAA	9128
F		6578-6603	CACC	
CytbR		15731-15750	AGAATGAGGAGGTCTGCGGC	

The names, gene, nucleotide positions, sequences and expected amplicon lengths of PCR primers used to generate the overlapping long-amplicons.

Table S3. Similarity of human sequences vs the homologous structural models used to analyse the effect mtDNA-encoded OXPHOS variations identified in breast-to-brain metastasis bloods. Complex III and IV similarities are reported elsewhere [1].

Complex I	<i>B. taurus</i> [PDB ID:5LC5]
Human Protein	Percentage Similarity
MT-ND1	78
MT-ND2	63
MT-ND3	73
MT-ND4	74
MT-ND4L	73
MT-ND5	70
MT-ND6	61

Complex V	<i>B. taurus</i> [PDB ID:5ARA]
Human Protein	Percentage Similarity
MT-ATP6	77
MT-ATP8	Not available

1
2
3
4
5
6
7
8
9
10
11
12
13
14
15
16
17
18
19
20
21
22
23
24
25
26
27
28
29
30
31
32
33
34
35
36
37
38
39
40
41
42
43
44
45
46
47
48
49

Table S4. Details of the mtDNA variation landscapes identified in breast-brain metastasis blood samples including location, average heteroplasmy and prevalence.

<i>Locus</i>	<i>Specific Nucleotide Variant</i>	<i>Amino Acid change</i>	<i>Average heteroplasmy (% ± SD)</i>	<i>% Prevalence in healthy population (Hmtdb)</i>	<i>Prevalence in patient samples (%)</i>	<i>Specific Sample IDs (BBM)</i>
D-loop	A73G	-	99.6±0.4	76.9	46.2	1/ 4/ 8/ 9/ 12/ 13
D-loop	A93G	-	13.2±0.0	2.5	7.7	6
D-loop	T146C	-	99.8±0.3	24.5	15.4	4/ 5
D-loop	C150T	-	99.6±0.6	10.6	15.4	1/ 10
D-loop	T152C	-	99.7±0.5	28.6	23.1	4/ 8/ 9
D-loop	A153G	-	99.6	3.6	7.7	5
D-loop	T195C	-	99.6	24.2	7.7	10
D-loop	A200G	-	97.2	2.4	7.7	2
D-loop	T217C	-	99.4±0.3	0.8	15.4	4/ 8
D-loop	C299A	-	14.5±1.8	0	23.1	4/ 5/ 12
D-loop	A301C	-	15.4±3.9	0	61.5	1/ 2/ 3/ 5/ 7/ 10/ 11/ 12
D-loop	A302AC	-	13.1±3.0	-	92.3	1/ 2/ 3/ 4/ 5/ 6/ 7/ 9/ 10/ 11/ 12/ 13

D-loop	<i>A302ACC</i>	-	2.8	-	7.7	8
D-loop	<i>C308T</i>	-	32±6.8	0	15.4	8/ 12
D-loop	<i>CT309C</i>	-	2.0	-	7.7	12
D-loop	<i>T310C</i>	-	75.7±4.0	5.1	100	All
D-loop	<i>T310TC</i>	-	18.2±4.5	-	100	All
D-loop	<i>T321C</i>	-	95.6	0.1	7.7	12
D-loop	<i>C340T</i>	-	94.8	0.4	7.7	8
D-loop	<i>C456T</i>	-	94.8	2.6	7.7	3
D-loop	<i>A492G</i>	-	14.4	0	7.7	5
D-loop	<i>A508G</i>	-	87.6±8.5	0.6	15.4	4/ 8
D-loop	<i>C510G</i>	-	12.8	0	7.7	8
D-loop	<i>A512C</i>	-	34.4	0.1	7.7	8
D-loop	<i>G513C</i>	-	26.4±7.7	0	15.4	3/ 10
D-loop	<i>GCA513G</i>	-	55.1±3.5	-	15.4	3/ 10
D-loop	<i>G513A</i>	-	41.2	1.5	7.7	8
D-loop	<i>G513GCA</i>	-	42.0	-	7.7	8
D-loop	<i>G564C</i>	-	24.0	0	7.7	4

1
2
3
4
5
6
7
8
9
10
11
12
13
14
15
16
17
18
19
20
21
22
23
24
25
26
27
28
29
30
31
32
33
34
35
36
37
38
39
40
41
42
43
44
45
46
47
48
49

D-loop	<i>C566A</i>	-	38.0	0	7.7	4
D-loop	<i>A567C</i>	-	42.3	0	7.7	4
D-loop	<i>A567AC</i>	-	42.8	-	7.7	4
D-loop	<i>A16051G</i>	-	95.4±0.3	2.6	15.4	4/ 8
D-loop	<i>T16092C</i>		93.2	1.3	7.7	4
D-loop	<i>T16093C</i>	--	92.4	5.6	7.7	8
D-loop	<i>C16111T</i>		100	2.7	7.7	5
D-loop	<i>T16126C</i>	-	100±0	11.9	15.4	1/ 12
D-loop	<i>G16129C</i>	-	98.4±0.6	0.6	15.4	4/ 8
D-loop	<i>G16129A</i>	--	99.8±0.3	15.8	15.4	5/ 7
D-loop	<i>G16153A</i>	-	100	0.9	7.7	1
D-loop	<i>CA16179C</i>	-	8.0±4.0	-	15.4	4/ 8
D-loop	<i>A16181AC</i>	-	8.4±2.9	-	15.4	4/ 8
D-loop	<i>A16182C</i>	-	70.8±3.4	7.5	15.4	4/ 8
D-loop	<i>A16183C</i>	-	65.3±40.7	13.6	23.1	4/ 6/ 8
D-loop	<i>A16183AC</i>	-	12.0	-	7.7	6
D-loop	<i>CT16188C</i>	-	8.8	-	7.7	6

D-loop	<i>T16189C</i>	-	98±0.3	29.6	15.4	4/ 8
D-loop	<i>C16192T</i>	-	98.8±0.6	4.0	15.4	9/ 13
D-loop	<i>C16234T</i>	-	99.2	3.5	7.7	2
D-loop	<i>C16256T</i>	-	98.1±2.8	3.6	30.8	5/ 8/ 9/ 13
D-loop	<i>A16258C</i>	-	98.4	0.3	7.7	8
D-loop	<i>C16270T</i>	-	92.8±8.5	5.3	15.4	9/ 13
D-loop	<i>C16291T</i>		98.8	2.8	7.7	1
D-loop	<i>C16294T</i>	-	98.4±2.3	9.3	15.4	1/ 12
D-loop	<i>C16296T</i>	-	98.8±0.6	2.4	15.4	1/ 12
D-loop	<i>T16304C</i>	-	99.2±0.6	6.2	15.4	3/ 12
D-loop	<i>T16311C</i>	-	99.3±0.6	23.6	23.1	2/ 11/ 12
D-loop	<i>A16316G</i>	--	99.6	1.0	7.7	7
D-loop	<i>C16320T</i>	-	99.6	2.4	7.7	5
D-loop	<i>T16362C</i>	-	99.3±0.6	16.0	23.1	3/ 4/ 8
D-loop	<i>A16399G</i>	-	100	2.6	7.7	9
D-loop	<i>T16519C</i>	-	98.9±1.0	66.9	53.8	1/ 4/ 5/ 6/ 7/ 10/ 12
D-loop	<i>G16526A</i>		98.4	1.1	7.7	13

RNR1	G709A	-	99.1±0.5	12.8	23.1	1/ 9/ 12
RNR1	G930A	-	99.2	2.2	7.7	12
RNR1	G988A	-	99.6	0.1	7.7	8
RNR2	A1811G	-	99.8±0.3	8.2	15.4	4/ 8
RNR2	G1888A	-	99.4±0.3	5.8	15.4	1/ 12
RNR2	A2581G	-	100	0.3	7.7	5
RNR2	A2706G	-	98.7±0.6	77.0	61.5	1/ 2/ 4/8/ 9/ 11/ 12/ 13
RNR2	G3010A	-	99.2	16.2	7.7	6
RNR2	AC3105A	-	56.3±0.5	-	100	All
RNR2	A3105T	-	17.7±5.4	0	69.2	3/ 4/ 5/ 7/ 9/ 10/ 11/ 12/ 13
RNR2	T3197C	-	100±0.0	4.2	15.4	9/ 13
RNR2	G3226T	-	39.2	0	7.7	8
RNR2	T3229A	-	42.8	0	7.7	8
RNR2	T3229TA	-	54.8	-	7.7	8
MT-ND1	A3720G	Q138Q	99.6±0	0.6	15.4	4/ 8
MT-ND1	A3796G	T164A	99.6	0.6	7.7	6

MT-ND1	<i>G3849A</i>	L181L	99.6	0.4	7.7	4
MT-ND1	<i>C3992T</i>	T229M	99.2	0.8	7.7	10
MT-ND1	<i>A4024G</i>	T240A	99.2	0.7	7.7	10
MT-ND1	<i>A4191C</i>	P295P	99.6	0	7.7	8
MT-ND1	<i>T4216C</i>	Y304H	99.4±0.3	10.5	15.4	1/ 12
MT-ND2	<i>T4553C</i>	F28F	99.6	0.2	7.7	4
MT-ND2	<i>T4736C</i>	T89T	99.2	0.1	7.7	4
MT-ND2	<i>T4838C</i>	P123P	98.8	0	7.7	7
MT-ND2	<i>A4917G</i>	N150D	98.6±0.9	5.2	15.4	1/ 12
MT-ND2	<i>T5004C</i>	L179L	100	0.9	7.7	10
MT-ND2	<i>G5147A</i>	T226T	99.8±0.3	3.9	15.4	5/ 12
MT-ND2	<i>A5390G</i>	M307M	100±0.0	0.7	15.4	4/ 8
MT-ND2	<i>T5426C</i>	H319H	99.6±0.6	0.9	15.4	4/ 8
MT-ND4	<i>A10876G</i>	L39L	99.8±0.3	1.1	15.4	4/ 8
MT-ND4	<i>A11251G</i>	L164L	99.4±0.9	9.8	15.4	1/ 12
MT-ND4	<i>T11353C</i>	A198A	99.6	0.2	7.7	9
MT-ND4	<i>A11467G</i>	L236L	98.7±1.2	13.5	30.8	4/ 8/ 9/ 13

MT-ND4	G11719A	G320G	99.1±0.8	75.3	53.8	1/ 4/ 7/ 8/ 9/ 12/ 13
MT-ND4	A11812G	L351L	99.2±0.0	3.6	15.4	1/ 12
MT-ND4L	C10619T	N50N	99.6	0.1	7.7	13
MT-ND5	G12372A	L12L	99.4±1	14.3	30.8	4/ 8/ 9/ 13
MT-ND5	A12397G	T21A	99.6	0.5	7.7	5
MT-ND5	C12557T	T74I	98.4	0.3	7.7	4
MT-ND5	T13020C	G228G	99.2±1.1	1.1	15.4	4/ 8
MT-ND5	G13368A	G344G	99.4±0.3	5.3	15.4	1/ 12
MT-ND5	A13419T	G361G	22.0	0	7.7	13
MT-ND5	T13617C	I427I	99.8±0.3	4.1	15.4	9/ 13
MT-ND5	T13734C	F466F	99.0±0.3	0.6	15.4	4/ 8
MT-ND5	G13813A	V493I	99.6	0.1	7.7	5
MT-ND5	G13889A	C518Y	99.6	0.1	7.7	10
MT-ND5	A14145G	T603T	98.8	0	7.7	11
MT-ND6	A14233G	D147D	99.2±0.6	3.9	15.4	1/ 12
MT-ND6	C14365T	V103V	99.2	0.6	7.7	10
MT-ND6	A14582G	V31A	99.6	0.6	7.7	10

MT-CYB	<i>C14766T</i>	T7I	98.9±0.8	74.9	46.2	1/ 4/ 8/ 9/ 12/ 13
MT-CYB	<i>A14793G</i>	H16R	99.6±0.0	2.3	15.4	9/ 13
MT-CYB	<i>T14819TTCTATA</i>	S25	2.4	-	7.7	12
MT-CYB	<i>G14905A</i>	M53M	98.4±0.6	5.5	15.4	1/ 12
MT-CYB	<i>A15218G</i>	T158A	100±0.0	2.0	7.7	9
MT-CYB	<i>C15452A</i>	L236I	99.4±0.9	9.8	15.4	1/ 12
MT-CYB	<i>T15461C</i>	L239L	100±0.0	0	7.7	12
MT-CYB	<i>A15607G</i>	K287K	99.0±0.9	5.5	15.4	1/ 12
MT-CYB	<i>C15661T</i>	P305P	99.6±0.0	0.1	7.7	8
MT-CYB	<i>C15833T</i>	L363L	99.2±0.0	0.7	7.7	3
MT-CO1	<i>C6045T</i>	L48L	99.8±0.3	0.6	15.4	4/ 8
MT-CO1	<i>T6152C</i>	V83V	99.4±0.3	0.7	15.4	4/ 8
MT-CO1	<i>G6267A</i>	A122T	98.8	0.2	7.7	2
MT-CO1	<i>T6776C</i>	H291H	99.2	2.2	7.7	5
MT-CO1	<i>C7028T</i>	A375A	99.4±0.6	78.6	61.5	1/ 2/ 4/ 8/ 9/ 11/ 12/ 13
MT-CO2	<i>T8265C</i>	L227P	24.8	0	7.7	4
MT-CO2	<i>A8266C</i>	L227L	32.0	0	7.7	4

MT-CO2	T8267C	STOP>Q	27.6	0	7.7	4
MT-CO2	TAGC8267T	STOP	3.7	-	7.7	4
MT-CO2	A8268T	STOP>L	26.1	0	7.7	4
MT-CO2	G8269C	STOP>Y	39.4	1.4	7.7	4
MT-CO2	G8269A	STOP>STOP	99.6	0	7.7	10
MT-CO3	C9469T	T88I	100	0.1	7.7	13
MT-CO3	G9477A	V91I	99.8±0.3	4.2	15.4	9/ 13
MT-CO3	A9664G	E153G	98.8	0.1	7.7	4
MT-CO3	A9667G	N154S	99.2	0.7	7.7	9
MT-CO3	T9845C	T213T	99.6	0.1	7.7	8
MT-ATP6	C8622A	P32P	99.6	0	7.7	8
MT-ATP6	G8697A	M57M	99.8±0.3	4.9	15.4	1/ 12
MT-ATP6	T8821C	S99P	83.2	0	7.7	2
MT-ATP6	G8989A	A155T	97.2	0	7.7	12
MT-ATP6	G8994A	L156L	100	2.2	7.7	11
MT-ATP6	G9123A	L199L	100	6.1	7.7	10
MT-ATP8	T8473C	P36P	99.2	1.1	7.7	4

MT-OLR	G5746A	-	96.8	0.1	7.7	2
NC	T5892A	-	31.6	0	7.7	8
NC	A5894C	-	42.4	0.1	7.7	8
NC	A5894ACC	-	50.0	-	7.7	8
NC	C8270T	-	34.1	0.4	7.7	4
NC	C8270CACCCCCTCT	-	28.9	-	7.7	4
NC	T8277TCTACCCCCC	-	2.4	-	7.7	4
MT-TQ	T4336C	-	99.6	1.1	7.7	3
MT-TM	A4435G	-	100	0.1	7.7	4
MT-TR	T10463C	-	99.4±0.3	5.0	15.4	1/ 12
MT-TL2	A12308G	-	99.0±0.5	13.5	30.8	4/ 8/ 9/ 13
MT-TT	A15907G	-	99.8±0.3	0.6	15.4	4/ 8
MT-TT	G15928A	-	99.6±0.6	5.1	15.4	1/ 12

Abbreviations: ND - NADH dehydrogenase subunit, CYB - Cytochrome Bc1 complex subunit, CO - Cytochrome C oxidase subunit, ATP - ATP synthase subunit, OLR - Origin of light strand replication, RNR - Ribosomal RNA gene, HmtDB - Human mitochondrial database

Table S5. Reported disease associations of each mtDNA variation identified from breast-to-brain metastasis patient bloods, as listed in MITOMAP (Green) and the human mitochondrial database (black)(date accessed 25th of October 2016).

Locus/ Human Subunit (Gene)	Human Nucleotide Change (Amino Acid Change)	Disease Association
D-loop	A73G	Thyroid tumours/ Prostate tumours
	A93G	Thyroid cancer/ Breast cancer
	T146C	Elderly fibroblasts/ Elderly & AD brains/ Prostate tumour/Ovarian carcinoma/ POLG/PEO
	C150T	Elderly fibroblasts & leukocytes/ Lung tumour/ Thyroid tumour/ Prostate tumours/Leukocytes/ Lung cancer/ Thyroid cancer/ Prostate cancer/ Oesophageal cancer/ MELAS/Obesity/Leber Hereditary Optic Neuropathy/Oncocytic pituitary adenoma/Gastric carcinoma/Colorectal cancer/Cardiomyopathy/Alzheimer/Noonan syndrome/Epilepsy/Neuropathy/ Ataxia and retinitis pigmentosa/Schizophrenia/Diabetes/Mitochondrial disease/Glaucoma/GBM/Oral squamous cell carcinoma/Serous Ovarian Cancer
	T152C	Elderly brains/ Elderly fibroblasts/ Ovarian carcinoma/ Breast tumour
	A153G	Thyroid tumor/Parkinson`s Disease/ Alzheimer's Disease/Diabetes/Obesity/Oncocytic pituitary adenoma/Endometrial carcinoma/Prostate cancer/Schizophrenia and bipolar disorder/Noonan syndrome/Cardiomyopathy/Leber hereditary optic neuropathy/Breast cancer/Esophageal cancer/Epilepsy/GBM
	T195C	Bipolar disorder/ Elderly/AD brains/ Lung tumour/ Thyroid tumour/ Ovarian tumour/ Prostate tumour/ Glioblastoma/ Melanoma
	A200G	Renal oncocytoma/Gastric cancer/Colorectal cancer/Cardiomyopathy/Schizophrenia and bipolar disorder/Glioma/Breast cancer/Mitochondrial disease/Glaucoma/Leber hereditary optic neuropathy/Lung cancer/GBM/Diabetes
	T217C	Thyroid tumors/Chronic periodontitis/Schizophrenia and bipolar disorder/Esophageal cancer/Diabetes/Mitochondrial disease/Leber hereditary optic neuropathy/Epilepsy
	C299A	None
	A301C	None
	A302insC	None
	A302insCC	None
	C308T	Diabetes type2/Glioma/ Noonan syndrome
	CT309C	
	T310C	Melanoma/ Thyroid tumor/Renal oncocytoma/Alzheimer/Endometrial carcinoma/Parotid carcinoma/Oncocytic pituitary

	adenoma/Schizophrenia and bipolar disorder/Cardiomyopathy/Epilepsy/Esophageal cancer/GBM/Diabetes/Ovarian endometrioidserous Ovarian Cancer
<i>T310insC</i>	None
<i>T321C</i>	Diabetes
<i>C340T</i>	Glioma/ Thyroid tumour/ Rhinopharinx ococytoma/ Schozoaffective disorder/ LHON/ GBM
<i>C456T</i>	Thyroid tumour/ Breast cancer/ Prostate cancer/ Renal oncocyoma/ Oncocytic pituitary adenoma/ Endometrial cancer type I/ Invasive mammary carcinoma/ Invasive primary mammary carcinoma/ Parotid carcinoma/ Serous ovarian cancer/ GBM/ Oral squamous cell carcinoma/ Parkinson's disease/ Diabetes type 2/ Obesity/ Chronic periodontitis/ Alzheimer's disease/ Schizophrenia/ Bipolar disorder type 1/ Noonan syndrome/ Mental disorder/ LHON/ Meningococcal disease
<i>A492G</i>	None
<i>A508G</i>	Thyroid tumor/Rhinopharinx oncocyoma/Chronic periodontitis/Schizophrenia and bipolar disorder/Esophageal cancer/Neuropathy/ Ataxia and retinitis pigmentosa (NARP)/ Fatal childhood maternally inherited Leigh's syndrome/Mitochondrial disease/Leber hereditary optic neuropathy/Diabetes
<i>C510G</i>	None
<i>A512C</i>	None
<i>G513C</i>	None
<i>GCA513G</i>	None
<i>G513A</i>	None
<i>G513insCA</i>	None
<i>G564C</i>	None
<i>C566A</i>	None
<i>A567C</i>	Ovarian tumour
<i>A567insC</i>	Ophthalmoplegia/ TWINKLE/PEO
<i>A16051G</i>	Thyroid tumor/Diabetes/Rhinopharinx oncocyoma/Chronic periodontitis/OXPHOS system deficiency/Schizophrenia and bipolar disorder/Noonan syndrome/Diabetes/Leber hereditary optic neuropathy/GBM
<i>T16092C</i>	Leber hereditary optic neuropathy/Gastric cancer/Alzheimer's disease/Diabetes/Prostate cancer/Non-syndromic optic neuropathy /Schizophrenia/Parkinson's Disease/Esophageal cancer/Epilepsy/Meningococcal disease/GBM
<i>T16093C</i>	None
<i>C16111T</i>	Parkinson's Disease/ Alzheimer's Disease/Diabetes/Obesity/Leber hereditary optic neuropathy/Schizophrenia/Prostate cancer
<i>T16126C</i>	Glioblastoma/ Thyroid tumor/Leber hereditary optic neuropathy/Renal oncocyoma/Parkinson's Disease/ Alzheimer's Disease/Diabetes/Chronic

	Progressive External Ophthalmoplegia/Oncocytic pituitary adenoma/Salivary mixed tumor/Tongue carcinoma/Warthin tumor/Chronic periodontitis/Prostate cancer/Endometrial carcinoma/Schizophrenia and bipolar disorder/Noonan syndrome/Breast cancer/Cardiomyopathy/Epilepsy/Non-syndromic optic neuropathy/Esophageal cancer/Glaucoma/Neurofibromatosis/Meningococcal disease/GBM/Ovarian cancer
G16129C	None
G16129A	None
G16153A	Thyroid tumor/Leber hereditary optic neuropathy/Prostate cancer/Oncocytic pituitary adenoma/Esophageal cancer/Diabetes/GBM
16179del2	None
CA16179C	None
A16181insC	None
A16182C	Prostate tumour/ Myoclonic Epilepsy and Ragged Red Muscle Fibers/Parkinson`s Disease/ Alzheimer's Disease/Diabetes/Schizophrenia/Breast cancer/Gastric cancer/Colorectal cancer/Leber hereditary optic neuropathy/MELAS/Schizophrenia and bipolar disorder/Noonan syndrome/Cardiomyopathy/Neurogenic muscle weakness/ Ataxia/ And Retinitis Pigmentosa/Maternally Inherited Syndrome/Cardiomyopathy/Esophageal cancer
A16183C	Lung tumour back-mutation/ Prostate tumour/ Thyroid tumor/Myoclonic Epilepsy and Ragged Red Muscle Fibers/Parkinson`s Disease/ Alzheimer's Disease/Diabetes/Breast cancer/Pituitary adenoma/Warthin tumor/Gastric cancer/Chronic periodontitis/MELAS/Colorectal cancer/Prostate cancer/Leber hereditary optic neuropathy/Endometrial carcinoma/Prostate cancer/Schizophrenia and bipolar disorder/Hypertension/Noonan syndrome/Breast cancer/Cardiomyopathy/Neurogenic muscle weakness/ Ataxia/ And Retinitis Pigmentosa/Maternally Inherited Syndrome/Esophageal cancer/Lung cancer/GBM/Ovarian cancer
A16183insC	None
16188del1	None
T16189C	Diabetes/ Melanoma/ Prostate tumour/NIDDM / Cardiomyopathy / Endometrial cancer risk / Mtdna copy number / Metabolic Syndrome
C16192T	Thyroid tumor/MELAS/Renal oncocytoma/Parkinson`s Disease/Diabetes/Obesity/Schizophrenia/Pituitary adenoma/Chronic periodontitis/Colorectal cancer/Prostate cancer/Leber hereditary optic neuropathy/Endometrial carcinoma/Noonan syndrome/Cardiomyopathy/Glioma/Esophageal cancer/GBM
C16234T	Thyroid tumor/Alzheimer's disease/Diabetes/Schizophrenia/Parkinson`s Disease/Obesity/Colorectal cancer/Prostate cancer/Endometrial carcinoma/Leber hereditary optic neuropathy/Esophageal cancer
C16256T	Thyroid tumor/MELAS/Renal oncocytoma/Pituitary adenoma/Parkinson`s Disease/Diabetes/Obesity/Gastric cancer/Prostate cancer/Alzheimer's

	disease/Endometrial carcinoma/Noonan syndrome/Breast cancer/Cardiomyopathy/Leber's hereditary optic neuropathy/Neurogenic muscle weakness/ Ataxia/ And Retinitis Pigmentosa/Maternally Inherited Syndrome/Esophageal cancer/Epilepsy/GBM/Meningococcal disease
A16258C	None
C16270T	Thyroid tumor/MELAS/Renal oncocytoma/Colorectal cancer/Prostate cancer/Endometrial carcinoma/Pituitary adenoma/Glioma/Noonan syndrome/Cardiomyopathy/Leber hereditary optic neuropathy/Diabetes/Mitochondrial encephalopathy with lactic acidosis and stroke-like episodes/Glaucoma/Epilepsy/GBM
C16291T	Thyroid tumor/Parkinson`s Disease/ Alzheimer's Disease/Diabetes/Obesity/Schizophrenia/Gastric cancer/Leber hereditary optic neuropathy/Endometrial carcinoma/Epilepsy/Glioma/Esophageal cancer/Neurofibromatosis/Lung cancer/Meningococcal disease/GBM/Serous Ovarian Cancer
C16294T	Thyroid tumor/Parkinson`s Disease/ Alzheimer's Disease/Diabetes/Obesity/Schizophrenia/Renal oncocytoma/Leber hereditary optic neuropathy/Pituitary adenoma/Tongue carcinoma/ Salivary mixed tumor/Warthin tumor/Prostate cancer/Endometrial carcinoma/Schizophrenia and bipolar disorder/Noonan syndrome/Cardiomyopathy/Breast cancer/Neurogenic muscle weakness/ Ataxia/ And Retinitis Pigmentosa/Maternally Inherited Syndrome/Glaucoma/Neurofibromatosis/Epilepsy/GBM/Serous Ovarian Cancer
C16296T	Thyroid tumor/Renal oncocytoma/Leber hereditary optic neuropathy/Pituitary adenoma/Tongue carcinoma/ Salivary mixed tumor/Warthin tumor/Prostate cancer/Schizophrenia and bipolar disorder/Noonan syndrome/Breast cancer/Diabetes/GBM
T16304C	Esophageal/ Breast & prostate tumours/ Thyroid tumor/Parkinson`s Disease/ Alzheimer's Disease/Diabetes/Obesity/Schizophrenia/Renal oncocytoma/Leber hereditary optic neuropathy/Pituitary adenoma/Parotid carcinoma/Warthin tumor/Gastric cancer/Chronic periodontitis/Colorectal cancer/Prostate cancer/Endometrial carcinoma/Esophageal cancer/Maternally inherited essential hypertension/Noonan syndrome/Periodic paralyses and neuropathy/Lung cancer/Meningococcal disease/Epilepsy/GBM/Serous Ovarian Cancer
T16311C	Prostate tumour
A16316G	Parkinson`s Disease/ Alzheimer's Disease/Diabetes/Obesity/Leber hereditary optic neuropathy/Schizophrenia/Esophageal cancer/Epilepsy/Oral squamous cell carcinoma
C16320T	Thyroid tumor/Renal oncocytoma/Chronic periodontitis/Diabetes/Obesity/Alzheimer's disease/Prostate cancer/Warthin tumor/Schizophrenia and bipolar disorder/Leber Hereditary Optic Neuropathy/OXPHOS system deficiency/Glaucoma/Meningococcal disease/Lung cancer

	T16362C	Thyroid tumor/Leber hereditary optic neuropathy/MELAS/Parkinson's Disease/ Alzheimer's Disease/Diabetes/Obesity/Rhinopharinx oncocytoma/Gastric cancer/Pituitary adenoma/Warthin tumor/Chronic periodontitis/Colorectal cancer/Prostate cancer/Ovarian cancer/Endometrial carcinoma/Schizophrenia and bipolar disorder/Hypertension/Noonan syndrome/Breast cancer/Cardiomyopathy/Neurogenic muscle weakness/ Ataxia/ And Retinitis Pigmentosa/Maternally Inherited Syndrome/Esophageal cancer/Glaucoma/Meningococcal disease/Lung cancer/Epilepsy/Oral squamous cell carcinoma/GBM/Serous Ovarian Cancer
	A16399G	Gastric carcinoma/ Thyroid tumor/MELAS/Parkinson's Disease/ Alzheimer's Disease/Diabetes/Obesity/Renal oncocytoma/Endometrial carcinoma/Prostate cancer/Noonan syndrome/Cardiomyopathy/Oncocytic pituitary adenoma/Leber hereditary optic neuropathy/Esophageal cancer/Glaucoma/Schizophrenia/Epilepsy/GBM/Non-syndromic Hearing loss/Oral squamous cell carcinoma
	T16519C	Glioblastoma/ Gastric/ Lung/ Ovarian/ Prostate tumours
	G16526A	Thyroid tumor/Prostate cancer/Leber hereditary optic neuropathy/Cardiomyopathy/Diabetes/Epilepsy/GBM
Mt-rnr1	G709A	None
	G930A	None
	G988A	Possible DEAF risk factor
Mt-rnr2	A1811G	Head/Neck tumour
	G1888A	None
	A2581G	Thyroid tumor/Prostate cancer/Leber hereditary optic neuropathy/OXPHOS system deficiency/Noonan syndrome/Diabetes
	A2706G	None
	G3010A	Cyclic Vomiting Syndrome with Migraine/ Thyroid tumor/Leber hereditary optic neuropathy/Renal oncocytoma/Obesity/Diabetes/Colorectal cancer/Prostate cancer/Pituitary adenoma/Parotid carcinoma/Endometrial carcinoma/OXPHOS system deficiency/Subcortical infarcts and leukoencephalopathy/Alivary benign neoplasia/Schizophrenia and bipolar disorder/Noonan syndrome/Cardiomyopathy/Breast cancer/Non-syndromic optic neuropathy /Esophageal cancer/Diabetes/Glaucoma/Periodic paralyses and neuropathy/Neurofibromatosis/Meningococcal disease/Lung cancer/Epilepsy/GBM/Ovarian endometrioid/Serous Ovarian Cancer
	AC3105A	None
	A3105T	None
	T3197C	None
	G3226T	None
	T3229A	None
	T3229insA	None

Mt-nd1

A3720G (Q138Q)	Thyroid tumor/Chronic periodontitis/Parkinson's Disease/Rhinopharinx oncocytoma/Schizophrenia and bipolar disorder/OXPHOS system deficiency/Leber hereditary optic neuropathy/Neurogenic muscle weakness/ Ataxia/ And Retinitis Pigmentosa/Maternally Inherited Syndrome/GBM/Diabetes
A3796G (T164A)	Adult-onset dystonia/ Prostate cancer/OXPHOS deficiency/Subcortical infarcts and leukoencephalopathy (CADASIL)/Schizophrenia and bipolar disorder/Diabetes
G3849A (L181L)	Chronic periodontitis/OXPHOS deficiency/Noonan syndrome/Esophageal cancer/Diabetes
C3992T (T229M)	Thyroid tumour/PD/ Thyroid tumour/Renal oncocytoma/Parotid oncocytoma/Endometrial carcinoma/Pituitary adenoma/OXPHOS deficiency/Noonan syndrome /Parotid carcinoma/Diabetes/GBM
A4024G (T240A)	PD/ Thyroid tumor/Renal oncocytoma/Parotid oncocytoma/Endometrial carcinoma/Pituitary adenoma/OXPHOS deficiency/Noonan syndrome /Parotid carcinoma/Diabetes/GBM
A4191C (P295P)	None
T4216C (Y304H)	PD/LHON/Insulin Resistance/Myelodysplastic syndromes/Acute leukemia/ Thyroid tumor/Leber hereditary optic neuropathy/Renal oncocytoma/Alzheimer/Diabetes/Pituitary adenoma/Prostate cancer/Endometrial carcinoma/OXPHOS deficiency/Subcortical infarcts and leukoencephalopathy/Schizophrenia and bipolar disorder/Noonan syndrome/Breast cancer/Cardiomyopathy/Epilepsy/Optic atrophy/Glaucoma/Neurofibromatosis/GBM/ Serous Ovarian Cancer

Mt-nd2

T4553C (F28F)	Chronic periodontitis/OXPHOS system deficiency/Diabetes
T4736C (T89T)	OXPHOS system deficiency/Schizophrenia and bipolar disorder/Parkinson's Disease/Leber hereditary optic neuropathy/Diabetes/Alzheimer's Disease
T4838C (P123P)	Diabetes
A4917G (N150D)	LHON / Insulin Resistance / Age-related macular degeneration / NRTI-PN/ Thyroid tumor/Renal oncocytoma/Leber hereditary optic neuropathy/Prostate cancer/Endometrial carcinoma/Tongue carcinoma/Oncocytic pituitary adenoma/OXPHOS system deficiency/Schizophrenia and bipolar disorder/Noonan syndrome/Cardiomyopathy/Epilepsy/Leber's hereditary optic neuropathy/Diabetes/Breast cancer/Neurofibromatosis/GBM/Serous Ovarian Cancer

	<i>T5004C</i> (L179L)	Thyroid tumor/Alzheimer's Disease/Renal oncocytoma/Diabetes/Pituitary adenoma/Parotid carcinoma/OXPHOS system deficiency/Noonan syndrome/Endometrial cancer
	<i>G5147A</i> (T226T)	Thyroid tumor/Renal oncocytoma/Obesity/Gastric cancer/ Oncocytic pituitary adenoma/Leber hereditary optic neuropathy/Endometrial carcinoma/OXPHOS system deficiency/Salivary mixed tumor/Warthin tumor/Parotid oncocytoma/Epilepsy/Noonan syndrome/Breast cancer/Schizophrenia/Esophageal cancer/Glaucoma/Lung cancer/GBM/Diabetes
	<i>A5390G</i> (M307M)	Thyroid tumor/Rhinopharinx oncocytoma/Chronic periodontitis/OXPHOS system deficiency/Subcortical infarcts and leukoencephalopathy/Schizophrenia and bipolar disorder/Neurogenic muscle weakness/ Ataxia/ And Retinitis Pigmentosa/Maternally Inherited Syndrome/Diabetes/Leber hereditary optic neuropathy
	<i>T5426C</i> (H319H)	Thyroid tumor/Rhinopharinx oncocytoma/Chronic periodontitis/OXPHOS system deficiency/Subcortical infarcts and leukoencephalopathy/Schizophrenia and bipolar disorder/Neurogenic muscle weakness/ Ataxia/ And Retinitis Pigmentosa/Maternally Inherited Syndrome /Esophageal cancer/Diabetes/Leber hereditary optic neuropathy/Epilepsy/GBM
<i>Mt-nd4</i>	<i>A10876G</i> (L39L)	Thyroid tumor/Rhinopharinx oncocytoma/Chronic periodontitis/OXPHOS system deficiency/Subcortical infarcts and leukoencephalopathy/Schizophrenia and bipolar disorder/Cardiomyopathy/Esophageal cancer/Diabetes/Leber hereditary optic neuropathy/GBM
	<i>A11251G</i> (L164L)	Thyroid tumor/Leber hereditary optic neuropathy/Renal oncocytoma/Chronic Progressive External Ophthalmoplegia/Pituitary adenoma/Tongue carcinoma/Salivary mixed tumor/Warthin tumor/Parotid oncocytoma/Endometrial carcinoma/Prostate cancer/OXPHOS system deficiency/Subcortical infarcts and leukoencephalopathy/Schizophrenia and bipolar disorder/Noonan syndrome/Breast cancer/Cardiomyopathy/Epilepsy/Non-syndromic optic neuropathy/Diabetes/Glaucoma/Neurofibromatosis/Serous Ovarian Cancer/GBM
	<i>T11353C</i> (A198A)	GBM/Cardiomyopathy/Leber's hereditary optic neuropathy
	<i>A11467G</i> (L236L)	Altered brain ph/ Thyroid tumor/MELAS/Renal oncocytoma/Leber hereditary optic neuropathy/Rhinopharinx oncocytoma/Pituitary adenoma/Oral cavity carcinoma/Warthin tumor/Chronic periodontitis/Prostate cancer/Endometrial carcinoma/OXPHOS system deficiency/Subcortical infarcts and leukoencephalopathy/Schizophrenia and bipolar disorder/Gliomas/Noonan syndrome/Breast cancer/Cardiomyopathy/Non-syndromic hearing loss/Autosomal dominant opticatrophy/Neurogenic muscle weakness/ Ataxia/ And Retinitis Pigmentosa/Maternally Inherited

		Syndrome/Diabetes/Neurofibromatosis/Epilepsy/GBM/Serous Ovarian Cancer
	<i>G11719A</i> (G320G)	None
	<i>A11812G</i> (L351L)	Thyroid tumor/Renal oncocytoma/ Leber hereditary optic neuropathy/Oncocytic pituitary adenoma/Salivary mixed tumor/Tongue carcinoma/Warthin tumor/Prostate cancer/Endometrial carcinoma/OXPHOS system deficiency/Schizophrenia and bipolar disorder/Noonan syndrome/Cardiomyopathy/Epilepsy/Breast cancer/Diabetes/GBM/ Oral squamous cell carcinoma/Serous Ovarian Cancer
<i>Mt-nd4L</i>	<i>C10619T</i> (N50N)	Thyroid tumor/Diabetes/Oral squamous cell carcinoma
<i>Mt-nd5</i>	<i>G12372A</i> (L12L)	Altered brain pH/Prostate tumour/ Thyroid cancer/Breast cancer/MELAS/Obesity/Renal oncocytoma/Leber Hereditary Optic/Chronic Periodontitis Neuropathy/Warthin tumor/Colorectal cancer/Endometrial cancer type I/OXPHOS system deficiency/Cerebral arteriopathy with subcortical infarcts and leukoencephalopathy/Schizophrenia/Neurofibromatosis type 1/Leber Hereditary Optic Neuropathy/Noonan syndrome/Autosomal dominant optic atrophy/Diabetes/Periodic paralyses and neuropathy/Hearing loss/Meningococcal disease/Serous Ovarian Cancer/Epilepsy
	<i>A12397G</i> (T21A)	Early-onset PD/ Thyroid tumor/Endometrial carcinoma/GBM/Diabetes/OXPHOS system deficiency/Parkinson's Disease/Tongue carcinoma
	<i>C12557T</i> (T74I)	Chronic periodontitis/Pituitary adenoma/OXPHOS system deficiency/Glaucoma/Leber hereditary optic neuropathy/Diabetes
	<i>T13020C</i> (G228G)	Thyroid tumor/Rhinopharynx oncocytoma/Chronic periodontitis/OXPHOS system deficiency/Subcortical infarcts and leukoencephalopathy/Schizophrenia and bipolar disorder/Neurogenic muscle weakness/ Ataxia/ And Retinitis Pigmentosa/Maternally Inherited Syndrome/Diabetes/Leber hereditary optic neuropathy/GBM
	<i>G13368A</i> (G344G)	Thyroid tumor/Leber hereditary optic neuropathy/Renal clear cell carcinoma/Chronic periodontitis/Prostate cancer/Endometrial carcinoma/OXPHOS system deficiency/Pituitary adenoma/Tongue carcinoma/Salivary mixed tumor/Warthin tumor/Parotid oncocytoma/Subcortical infarcts and leukoencephalopathy/Schizophrenia and bipolar disorder/Glioma/Noonan syndrome/Cardiomyopathy/Epilepsy/Breast cancer/Diabetes/Neurofibromatosis/GBM/Serous Ovarian Cancer
	<i>A13419T</i> (G361G)	Non-syndromic Hearing loss
	<i>T13617C</i> (I427I)	Thyroid tumor/MELAS/Renal oncocytoma/ Diabetes/Pituitary adenoma/Prostate cancer/Endometrial carcinoma/OXPHOS system

		deficiency/Subcortical infarcts and leukoencephalopathy/Glioma/Noonan syndrome/Cardiomyopathy/Leber's hereditary optic neuropathy/Diabetes/Epilepsy/GBM/ Neurogenic muscle weakness/ Ataxia and retinitis pigmentosa/ Maternally inherited form of Leigh syndrome
	T13734C (F466F)	Thyroid tumor/ Renal oncocytoma/Chronic periodontitis/OXPHOS system deficiency/Rhinopharinx oncocytoma/Subcortical infarcts and leukoencephalopathy/Schizophrenia and bipolar disorder/Diabetes/Leber hereditary optic neuropathy/GBM
	G13813A (V493I)	None
	G13889A (C518Y)	Head/Neck tumour/ Parotid oncocytoma/Schizophrenia/Mitochondrial disease
	A14145G (T603T)	Prostate cancer
Mt-nd6	A14233G (D147D)	Thyroid tumor/Leber hereditary optic neuropathy/Prostate cancer/Endometrial carcinoma/Oncocytic pituitary adenoma/OXPHOS system deficiency/Schizophrenia and bipolar disorder/Tongue carcinoma/Noonan syndrome/Cardiomyopathy/Salivary mixed tumor/Breast cancer/Warthin tumor/Epilepsy/Esophageal cancer/Diabetes/GBM/Oral squamous cell carcinoma/Serous Ovarian Cancer
	C14365T (V103V)	Thyroid tumor/Renal oncocytoma/Endometrial carcinoma/OXPHOS system deficiency/Pituitary adenoma/Parotid carcinoma/Diabetes/Noonan syndrome
	A14582G (V31A)	Thyroid tumor/Renal oncocytoma/Endometrial carcinoma/Parkinson`s Disease/Pituitary adenoma/Parotid carcinoma/OXPHOS system deficiency/Noonan syndrome/Diabetes/GBM/ Ovarian endometrioid
Mt-cyb	C14766T (T7I)	None
	A14793G (H16R)	Thyroid tumor/Renal oncocytoma/MELAS/Prostate cancer/Endometrial carcinoma/Alzheimer's Disease/OXPHOS system deficiency/Subcortical infarcts and leukoencephalopathy/Noonan syndrome/Cardiomyopathy/Leber hereditary optic neuropathy/Diabetes/GBM/ Serous Ovarian Cancer
	T14819insTCTAT A	None
	G14905A (M53M)	Thyroid tumor/Renal oncocytoma/Leber hereditary optic neuropathy/Oncocytic pituitary adenoma/Salivary mixed tumor/ Warthin tumor/Gastric cancer/Prostate cancer/Endometrial carcinoma/OXPHOS system deficiency/Subcortical infarcts and leukoencephalopathy/Schizophrenia and bipolar disorder/Noonan

		syndrome/Cardiomyopathy/Epilepsy/Breast cancer/Diabetes/Glaucoma/Neurofibromatosis/GBM
	A15218G (T158A)	Thyroid tumor/Renal oncocytoma/MELAS/Leber hereditary optic neuropathy/Diabetes/Endometrial carcinoma/Prostate cancer/OXPHOS system deficiency/Noonan syndrome/Pituitary adenoma/Cardiomyopathy/Esophageal cancer/Neurogenic muscle weakness/ Ataxia/ And Retinitis Pigmentosa/Maternally Inherited Syndrome/Lung cancer/GBM
	C15452A (L236I)	Thyroid tumor/Leber hereditary optic neuropathy/Renal oncocytoma/Chronic Progressive External Ophthalmoplegia/Pituitary adenoma/Oncocytic pituitary adenoma/Salivary mixed tumor/Tongue carcinoma/Warthin tumor/Prostate cancer/Endometrial carcinoma/OXPHOS system deficiency/Subcortical infarcts and leukoencephalopathy/Schizophrenia and bipolar disorder/Noonan syndrome/Cardiomyopathy/Epilepsy/Breast cancer/Diabetes/Glaucoma/Neurofibromatosis/GBM/Ovarian cancer
	T15461C (L239L)	None
	A15607G (K287K)	Breast cancer/ Thyroid tumor/Renal oncocytoma/Leber hereditary optic neuropathy/Diabetes/Endometrial carcinoma/Prostate cancer/OXPHOS system deficiency/Subcortical infarcts and leukoencephalopathy/Schizophrenia and bipolar disorder/Noonan syndrome/Cardiomyopathy/Pituitary adenoma/Tongue carcinoma/ Salivary mixed tumor/Warthin tumor/Epilepsy/Breast cancer/Neurofibromatosis/GBM/Serous Ovarian Cancer
	C15661T (P305P)	Thyroid cancer
	C15833T (L363L)	Oncocytic pituitary adenoma/ Endometrial cancer type 1/ Noonan syndrome/ GBM/ Serous ovarian cancer
Mt-co1	C6045T (L48L)	Thyroid tumor/Rhinopharinx oncocytoma/Chronic periodontitis/OXPHOS system deficiency/Infarcts and leukoencephalopathy/Schizophrenia and bipolar disorder/Diabetes/Leber hereditary optic neuropathy/GBM
	T6152C (V83V)	Thyroid tumor/Rhinopharinx oncocytoma/Chronic periodontitis/Endometrial cancer/OXPHOS system deficiency/Subcortical infarcts and leukoencephalopathy/Bipolar disorder/Diabetes/Glaucoma/Leber hereditary optic neuropathy/GBM
	G6267A (A122T)	Prostate Cancer/Pancreatic cancer/ Leber hereditary optic neuropathy
	T6776C (H291H)	Breast cystic masses/ Thyroid tumor/Renal oncocytoma/Prostate cancer/OXPHOS system deficiency/Subcortical infarcts and leukoencephalopathy/Oncocytic pituitary adenoma/Schizophrenia and

	bipolar disorder/Glioma/Noonan syndrome/Breast cancer/Cardiomyopathy/Diabetes/Epilepsy/GBM/Serous Ovarian Cancer	
	C7028T (A375A)	None
Mt-co2	T8265C (L227P)	None
	A8266C (L227L)	None
	T8267C (STOP>Q)	None
	8267delAGC	None
	A8268T (STOP>L)	None
	G8269A (STOP>STOP)	Thyroid tumor/Renal oncocytoma/Pituitary adenoma/Parotid oncocytoma/Colorectal cancer/OXPHOS system deficiency/Noonan syndrome/Diabetes/GBM/ Ovarian cancer
	G8269C (STOP>Y)	None
Mt-co3	C9469T (T88I)	Diabetes
	G9477A (V91I)	Thyroid tumour/ Thyroid tumour/MELAS/Renal oncocytoma/Alzheimer's Disease/Parkinson`s Disease/Pituitary adenoma/Prostate cancer/Endometrial carcinoma/OXPHOS system deficiency/ Subcortical infarcts and leukoencephalopathy/Noonan syndrome/Glioma/Cardiomyopathy/Diabetes/Epilepsy/GBM
	A9664G (E153G)	Diabetes
	A9667G (N154S)	Thyroid tumor/ MELAS/Prostate cancer/Leber's hereditary optic neuropathy/Parkinson`s Disease/Diabetes/Epilepsy
	T9845C (T213T)	None
Mt-atp6	C8622A (P32P)	None
	G8697A (M57M)	Thyroid tumour/ Thyroid tumour/Renal oncocytoma/Leber hereditary optic neuropathy/Oncocytic pituitary adenoma/Tongue carcinoma/Salivary mixed tumor/Warthin tumor/Parotid oncocytoma/Prostate cancer/Endometrial carcinoma/OXPHOS system deficiency/Subcortical infarcts and leukoencephalopathy/Schizophrenia

		and bipolar disorder/Noonan syndrome/Cardiomyopathy/Epilepsy/Breast cancer/Diabetes/Neurofibromatosis/Leber hereditary optic neuropathy/GBM
	<i>T8821C</i> (S99P)	None
	<i>G8989A</i> (A155T)	Diabetes/Schizophrenia
	<i>G8994A</i> (L156L)	Thyroid tumor/Renal oncocyoma/Parkinson's Disease/Alzheimer's Disease/Chronic periodontitis/Oncocytic pituitary adenoma/Warthin tumor/Prostate cancer/OXPHOS system deficiency/Subcortical infarcts and leukoencephalopathy/Diabetes/Breast cancer/Epilepsy
	<i>G9123A</i> (L199L)	Thyroid tumor/Leber hereditary optic neuropathy/Renal oncocyoma/Alzheimer's Disease/Parkinson's Disease/Pituitary adenoma/Parotid carcinoma/Gastric cancer/Endometrial carcinoma/OXPHOS system deficiency/Noonan syndrome/Esophageal cancer/Diabetes
<i>Mt-atp8</i>	<i>T8473C</i> (P36P)	Chronic periodontitis/Obesity/Diabetes/Prostate cancer/Pituitary adenoma/OXPHOS system deficiency/Schizophrenia and bipolar disorder/Cardiomyopathy/Leber hereditary optic neuropathy/Esophageal cancer
<i>Mt-tq</i>	<i>T4336C</i>	AD/PD/ Hearing loss & migraine/ Breast cancer/ Glioma/ Oncocytic pituitary adenoma/ Endometrial cancer type I/ Alzheimer's disease/ Noonan syndrome/ Meningococcal disease
<i>Mt-tm</i>	<i>A4435G</i>	LHON modulator / Hypertension/ Leber hereditary optic neuropathy/Diabetes
<i>Mt-tr</i>	<i>T10463C</i>	Endometrium tumour/ Thyroid tumor/Renal oncocyoma/Leber hereditary optic neuropathy/Oncocytic pituitary adenoma/Tongue carcinoma/Salivary mixed tumor/Warthin tumor/Parotid oncocyoma/Prostate cancer/Endometrial carcinoma/OXPHOS system deficiency/ Subcortical infarcts and leukoencephalopathy/Schizophrenia and bipolar disorder/Noonan syndrome/Cardiomyopathy/Epilepsy/Breast cancer/Diabetes/Neurofibromatosis/Gbmserous Ovarian Cancer
<i>Mt-tl2</i>	<i>A12308G</i>	CPEO / Stroke / Cardiomyopathy / Breast & Renal & Prostate Cancer Risk / Altered brain ph/Lung & prostate tumour/ Thyroid cancer/Breast cancer/Serous Ovarian Cancer/Glioma/MELAS/Renal oncocyoma/Leber Hereditary Optic Neuropathy /Pituitary adenoma/Oral cavity carcinoma /Warthin tumor/Chronic Periodontitis/Prostate cancer/Endometrial cancer type I/Cerebral arteriopathy with subcortical infarcts and leukoencephalopathy/Schizoaffective disorder/Neurofibromatosis type 1/Noonan syndrome/Meningococcal disease/Epilepsy /Diabetes
<i>Mt-tt</i>	<i>A15907G</i>	Thyroid tumor/Chronic periodontitis/OXPHOS system deficiency/Rhinopharinx oncocyoma/Subcortical infarcts and leukoencephalopathy/Schizophrenia and bipolar

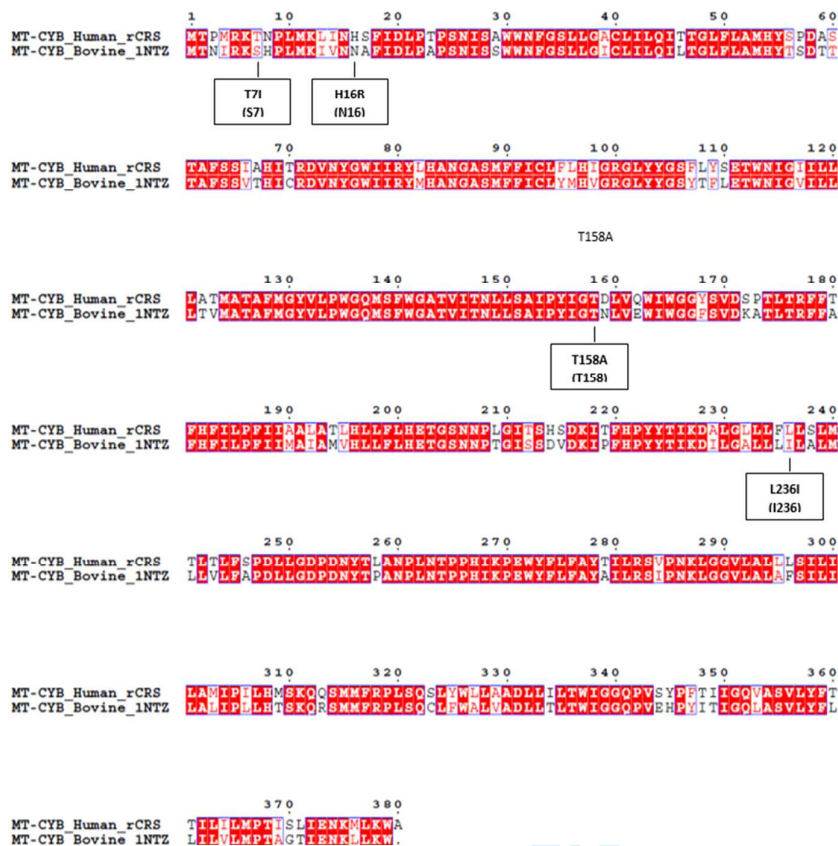
		disorder/Diabetes/Leber hereditary optic neuropathy/Neurogenic muscle weakness, ataxia and Retinitis Pigmentosa/Maternally Inherited Syndrome
	G15928A	Multiple Sclerosis / Idiopathic repeat miscarriage / AD protection/ Thyroid tumor/Renal oncocytoma/Diabetes/Leber hereditary optic neuropathy/Endometrial carcinoma/Prostate cancer/OXPHOS system deficiency/Subcortical infarcts and leukoencephalopathy/Schizophrenia and bipolar disorder/Noonan syndrome/Cardiomyopathy/Pituitary adenoma/Tongue carcinoma/ Salivary mixed tumor/Warthin tumor/Chronic periodontitis/Glioma/Epilepsy/Breast cancer/Esophageal cancer/Neurofibromatosis/GBM/Serous Ovarian Cancer
Mt-olr	G5746A	Chronic periodontitis/Diabetes/Leber hereditary optic neuropathy
Other non-coding regions	T5892A	None
	A5894C	Gastric carcinoma
	A5894CC	None
	C8270T (NC7)	Gastric cancer/Diabetes/Oncocytic pituitary adenoma/Mitochondrial disease/Epilepsy
	C8270insACCCC CTCT	None
	T8277insTCTAC CCCCC	None

Abbreviations: AD – Alzheimer’s disease/ PD – Parkinson’s disease/ Sporadic progressive external ophthalmoplegia/ DEAF - Maternally inherited deafness or aminoglycoside-induced deafness/ NTRI-PN - Antiretroviral Therapy-Associated Peripheral Neuropathy/ MELAS - Mitochondrial Encephalomyopathy Lactic Acidosis and Stroke like episodes/ CPEO - Chronic Progressive External Ophthalmoplegia.

Complex I



Complex III



1 10 20 30 40 50 60

MT-COI_2EIJ
MT-COI_Human_CRS

70 80 90 100 110 120

MT-COI_2EIJ
MT-COI_Human_CRS

130 140 150 160 170 180

MT-COI_2EIJ
MT-COI_Human_CRS

A122T
(A122)

190 200 210 220 230 240

MT-COI_2EIJ
MT-COI_Human_CRS

250 260 270 280 290 300

MT-COI_2EIJ
MT-COI_Human_CRS

310 320 330 340 350 360

MT-COI_2EIJ
MT-COI_Human_CRS

370 380 390 400 410 420

MT-COI_2EIJ
MT-COI_Human_CRS

430 440 450 460 470 480

MT-COI_2EIJ
MT-COI_Human_CRS

490 500 510

MT-COI_2EIJ
MT-COI_Human_CRS

MT-CO2_Human_CRS
 MT-CO2_Bovine_2EIJ

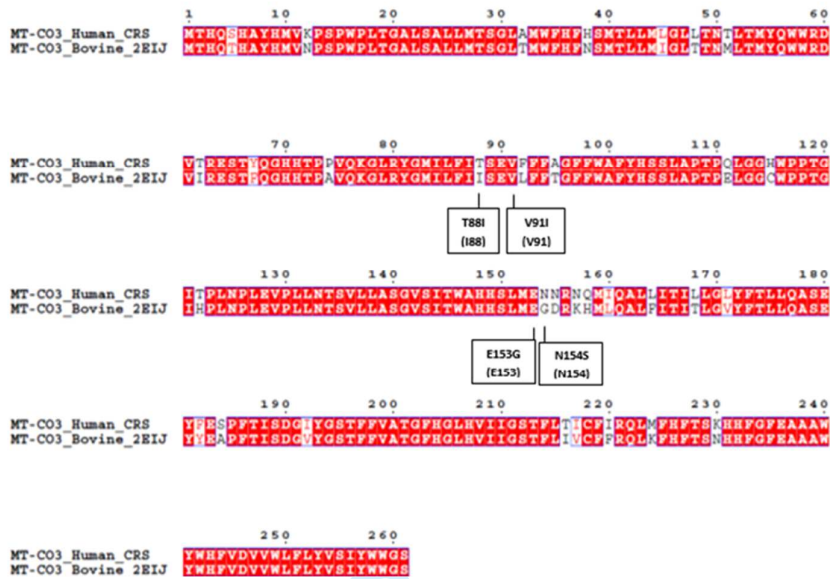
10 20 30 40 50 60
 MAHARQGLQDATSPIMEELIAPHDHALMIPLICFLVLYTALSLTLTKLTNTNISDAQRE
 MAYPMQGFQDATSPIMEELIAPHDHALMIPLISSLVLYTALSLMTLTKLTHSTMDAQRE

70 80 90 100 110 120
 METVNTILPAIILVLIALLPSLRILYMTDEVINDPSLTAKSHGHQWYWHYETTDYGGTIFNS
 VETVNTILPAIILVLIALLPSLRILYMDDEVINDPSLTAKSHGHQWYWHYETTDYEDTSFCS

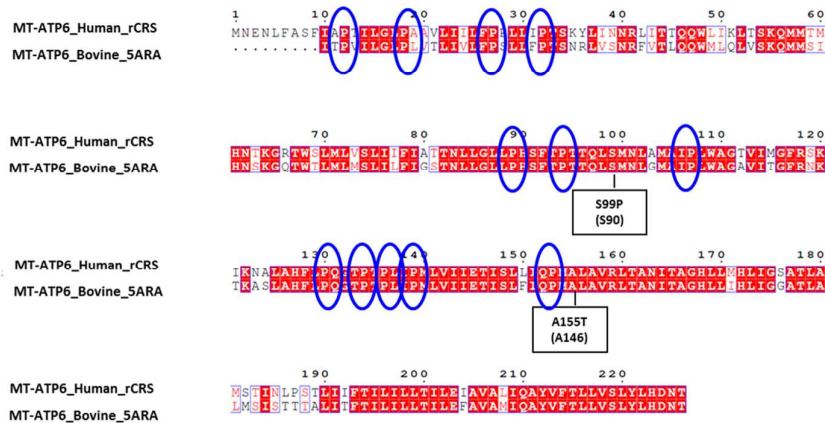
130 140 150 160 170 180
 YMHPLPLLEPGLELLRLVDNRRVVLPHETPIRMWITSQDVLHSAWVPLGLKLTDAIPGRLN
 YMHPLTSLKPGLELLRLVDNRRVVLPHETPIRMWITSQDVLHSAWVPLGLKLTDAIPGRLN

190 200 210 220
 OTTFATLRPGVYYGQCSEICGANNHSPMPIVLELPLKIFRMGRVFTT
 OTTLMSSRPGVYYGQCSEICGANNHSPMPIVLELPLKIFRMGRVFTT

L227P
(L227)



Complex V



Conserved prolines that relate to Figure 7 in the main text are highlighted in blue.

Figure S2. Comparison of the wild type *mt-cyb* and MT-CYB sequences against the variant sequences which contain a 6-nucleotide insertion at position 14819.

```
atgaccccaatacgcaaaactaaccccttaataaaatattaccactcattcatgac
M T P M R K T N P L M K L I N H S F I D
ctccccacccatccaacatctccgatgatgaacttcggctcactccttggcgctgc
L P T P S N I S A W W N F G S L L G A C
ctgactcctcaaatcaccagagactattcttagcctgactactcaccagagcgtcta
L I L Q I T T G L F L A M H Y S P D A S
accgcttttcatcaatcgccacatcactcgagagtaaatatgctgctgaatcctgc
T A F S S I A H I T R D V N Y G W I I R
taccttcacgccaatggcgctcaatattctttatctgctcttctacacatcgggoga
Y L H A N G A S M F F I C L F L H I G R
ggcttatattacggatcattctctcactcagaacctgaaacatcggtattatcctctg
G L Y Y G S F L Y S E T W N I G I L L
cttgcaactatagcaacagccttcataagctatgctcctccgtgaggccaatattc
L A T M A T A F M G Y V L P W G Q M S F
tgaggggccacagtaattacaacttactatccgcatcccatcattgggacagaccta
W G A T V I T N L L S A I P Y I G T D L
gttcaatgaatctgaggaggtactcagtagacgtccaccctcacagattctttacc
V Q W I W G G Y S V D S P T L T R F F T
tttcaacttcatcttgccttcattatgacgcttagcaacactccacctcctattctg
F H F I L P F I I A A L A T L H L L F L
cacgaaacgggatcaaacaccccttaggaatcactcccatccgatataatcaccttc
H E T G S N N F L G I T S H S D K I T F
caccttactacacatacaagagcgctcggttacttctcttctctctcttaag
H P Y Y T I K D A L G L L L F L L S L M
acattaacactattctcaccagacctcctaggcgacccagacattataccttagccaac
T L T L F S P D L L G D P D N Y T L A N
ccttaaacacccctccacacatcaaccccaatgatatttcttctcctcctacacatt
P L N T P P H I K P E W Y F L F A Y T I
ctcgatccgtcccttaacaaactagagggtcccttgcctattactatcctcctc
L R S V P N K L G G V L A L L S I L I
ctagcaataatccccatcctccatataccaacaacaaagcataatttgcgccaata
L A M I P I L H M S K Q Q S M M F R P L
agccaatcactttattgactccttagcgagacctcctcattcaactgaactggagga
S Q S L Y W L L A A D L L I L T W I G G
caaccagtaagctacccctttaccatcatggacaagtagatccgtactatcctcaca
Q P V S Y P P T I I G Q V A S V L Y F T
acaatcctaactcaataacacatctcctcaattgaaacaaaatactcaaatgggc
T I L I L M P T I S L I E N K M L K W A
t
```

Wild type

```
atgaccccaatacgcaaaactaaccccttaataaaatattaccactcattcatgac
M T P M R K T N P L M K L I N H S F I D
ctccccacccatctctataccaacatctccgatgatgaacttcggctcactccttggc
L P T P F Y T N I S A W W N F G S L L G
gctcgtcgtatcctccaatcaccagagactattcttagcctgactactcaccagac
A C L L Q I T T G L F L A M H Y S P D
gctcacaacggcttttcatcaatcgccacatcactcgagagtaaatatgctgctgaatc
A S T A F S S I A H I T R D V N Y G W I
atccgctaccttcacgccaatggcgctcaatattctttatctgctcctcctacacatc
I R Y L H A N G A S M F F I C L F L H I
ggcgagggcctatattacggatcatttctcactcagaacctgaaacatcggtcattatc
G R G L Y Y G S F L Y S E T W N I G I I
ctcctgctgcaactatagcaacagccttcataagctatgctcctccgtgaggccaata
L L L A T M A T A F M G Y V L P W G Q M
tcattctgagggggcacagtaattacaacttactatccgccatcccatcattgggaca
S F W G A T V I T N L L S A I P Y I G T
gacctagtccaatgaatctgaggaggtcactcagtagacagctccaccctcacagattc
D L V Q W I W G G Y S V D S P T L T R F
tttcaacttcaactccttgccttcattatgacgcttagcaacactccacctcctta
F T F H F I L P F I I A A L A T L H L L
ttcttgacgaaacgggatcaaacaccccttaggaatcactcccatccgatataatc
F L H E T G S N N P L G I T S H S D K I
accttcaaccttactacacatacaagagcgctcgtggtacttctctctctctctcc
F H P Y Y T I K D A L G L L L F L L S
ttaatgacattatacactatttccacagacctccttagcgacccagacattatacctta
L M T L T L F S P D L L G D P D N Y T L
gccaaaccccttaaacacccctccacacataagcccgatgatatttcttattcgctac
A N P L N T P P H I K P E W Y F L F A Y
acaattctcgtatccgtccatacaaaactagagggtccttgcctattactatcctc
F I L R S V P N K L G G V L A L L S I
ctcactagcaataatccccatcctccatataccaacaacaaagcataaatattgcg
L I L A M I P I L H M S K Q Q S M M F R
ccactaagccaatcactttattgactccttagcgagacctcctcatttcaacctgaatc
F L S Q S L Y W L L A A D L L I L T W I
ggaggaacacagtaagctacccctttaccatattggacaagtagatccgtactatac
G G Q P V S Y P P T I I G Q V A S V L Y
ttcacacaatcctaactcaataacacatctcctcaattgaaacaaaatactcaaaa
F T T I L I L M P T I S L I E N K M L K
tgggcct
W A
```

T14819insTCTATA Variant Sequence

References

1. Lloyd, R.E.; McGeehan, J.E. Structural Analysis of Mitochondrial Mutations Reveals a Role for Bigenomic Protein Interactions in Human Disease. *PLoS One*. 2013, 8, e69003.

For Peer Review Only